





Formulation Optimization, Physicochemical Characterization, and Biocompatibility Assessment of Curcumin-Loaded Aquasomes

¹Department of Pharmaceutics, Faculty of Pharmacy Nutrition and Dietetics, Lusaka Apex Medical University, Lusaka, Zambia | ²Department of Pharmaceutical Technology, Graduate School, Anadolu University, Eskisehir, Turkey | ³Department of Chemistry, Faculty of Science, Eskişehir Technical University (ESTU), Eskisehir, Turkey | ⁴Department of Pharmaceutical Technology, Faculty of Pharmacy, Anadolu University, Eskisehir, Turkey

Correspondence: Fernando Bwalya (fernando.bwalya@lamu.edu.zm)

Received: 19 September 2024 | Revised: 21 November 2024 | Accepted: 23 December 2024

Funding: The authors received no specific funding for this work.

Keywords: aquasome | biocompatibility | characterization | curcumin | QbD

ABSTRACT

Curcumin, a polyphenolic compound with numerous health benefits, suffers from poor aqueous solubility and low bioavailability, limiting its therapeutic potential. This study aimed to characterize and enhance curcumin's bioavailability by aquasomes (AQ)—a novel drug delivery system comprising a core, a carbohydrate layer, and the drug. Using a central composite design within the response surface methodology, formulation parameters—core-to-coat ratio, incubation time, and drug amount—were optimized to achieve the desired particle size, polydispersity index (PDI), and zeta potential. Hydroxyapatite (HAP) cores were coated with various sugars (lactose, sucrose, maltose, and trehalose) and loaded with curcumin, then characterized by size, zeta potential, encapsulation efficiency, thermogravimetric analysis, and Fourier-transform infrared spectroscopy (FTIR). The optimized HAP cores exhibited a particle size of 55.41 nm. Curcumin-loaded AQ showed larger sizes, with sucrose and maltose formulations measuring 215.6 and 329.5 nm, respectively. Encapsulation efficiencies ranged from 50% to 55.1%, with trehalose-coated AQ showing the highest efficiency. Drug release studies demonstrated a sustained release profile, with trehalose AQ achieving 90% release within 100 min. Stability assessments indicated no significant changes over 90 days, and photostability tests showed improved protection against light-induced degradation. The study developed curcumin-loaded AQ with enhanced stability and solubility, optimized through quality by design principles, offering a promising strategy to improve curcumin's bioavailability.

1 | Introduction

Curcumin is a polyphenolic compound found in the spice turmeric. It has various health benefits, including reducing inflammation, fighting oxidative stress, inhibiting cell growth, and antiangiogenic effects [1, 2]. Curcumin is classified as a Class IV drug in the (BCS); it has poor aqueous solubility and negligible permeability through the gastrointestinal epithelium [3]. Although Phase I clinical trials have demonstrated its safety

in humans even at high dosages (12 g/day), curcumin exhibits low bioavailability. This is primarily attributed to inadequate absorption, first-pass metabolism, and rapid elimination from the body [4, 5]. Thus, there is a need for enhanced delivery systems such as aquasomes (AQ) to improve curcumin's bioavailability.

AQ resemble "water bodies," and their water-like properties aid in safeguarding and preserving active pharmaceutical ingredients (APIs). These nanoparticles consist of a nanocrystalline core

This is an open access article under the terms of the Creative Commons Attribution License, which permits use, distribution and reproduction in any medium, provided the original work is properly cited.

© 2025 The Author(s). Nano Select published by Wiley-VCH GmbH.

enveloped by a carbohydrate layer, onto which drug moieties or other biochemical molecules can be adsorbed, either with or without modification [6]. AQ are among the most recently developed delivery systems for bioactive molecules like peptides, proteins, hormones, antigens and genes [7]. AQ' unique structure and properties enable the preservation of the conformational integrity and bioactivity of the encapsulated molecules, making them a promising drug delivery system for diverse therapeutic applications [8–15].

The quality by design (QbD) method is a strategy for developing drugs that guarantee the excellence of the result. This approach is centered on evaluating and managing the critical quality attributes (CQAs) of the product being developed [16]. The QbD approach is advantageous in early-developing aquasome drug delivery systems for curcumin delivery. The QbD methodology includes three main elements: characterizing the quality target product profile (QTPP), identifying the CQAs of the targeted product, evaluating the production method and defining the critical process parameters (CPPs). The first phase in the QbD process is gathering all prior research data that may impact the target product profile. The risk assessment (RA) application highlighted the features that influence the final aquasome formulation quality for IND after an early understanding of space design and evaluation of QTPPs, CQAs, and CPPs [16].

In optimizing formulations, the central composite design (CCD) is a foundational approach within response surface methodology (RSM) that facilitates a structured exploration of the interplay between multiple factors and responses. This method skillfully integrates factorial points, star points, and central points, enabling the comprehensive investigation of the factors' linear, interaction, and quadratic effects on the responses [17]. The strategic placement of star points allows for the efficient estimation of curvature, a feature that makes CCD particularly beneficial for uncovering and modeling nonlinear relationships between variables [17, 18].

Despite the potential of AQ as drug delivery systems, there is limited research on their application for improving the bioavailability of poorly soluble drugs like curcumin. Previous studies have neither extensively explored the optimization of aquasome formulations for curcumin nor compared the effects of different carbohydrate coatings on the physicochemical properties and drug release profiles. Therefore, this study aims to fill this gap by developing and optimizing curcumin-loaded AQ using various sugars as coatings and comprehensively characterizing their properties to assess their potential to enhance curcumin's bioavailability.

The objectives of this study are multifaceted, aiming to comprehensively explore the potential of AQ as an innovative nanoparticulate delivery system for enhancing the bioavailability of poorly soluble drugs. First, the study applies the QbD approach to identify and optimize critical process parameters that influence the formulation of curcumin-loaded AQ. Following this, a thorough physicochemical characterization of hydroxyapatite (HAP), sugar-coated HAP, and curcumin-loaded AQ was conducted to elucidate their structural and functional properties. The study also evaluated the in vitro release kinetics of curcumin from the aquasome formulations, focusing on the rate and mechanisms

of release. Additionally, the long-term stability of curcuminloaded AQ under various storage conditions, including light, temperature, and humidity was investigated. Finally, the biocompatibility using the hemolysis test was done to ensure the safety of curcumin-loaded AQ for clinical applications.

2 | Materials

Calcium chloride was obtained from Merck in Germany, disodium hydrogen phosphate was provided by Carlo Erba Reagents in Germany, and lactose monohydrate came from Drogsan in Turkey. Maltose was procured from Merck in Germany. Methanol, polyvinylpyrrolidone, potassium chloride, sodium chloride, and sucrose were supplied by Sigma Aldrich in Germany. Potassium dihydrogen phosphate was sourced from Sigma in the United States. Curcumin, sodium hydroxide, and Triton X-100 were acquired from Alko Argem Research and Development Centre, and trehalose was obtained from Sisco Research Laboratories Pvt. Ltd. in Turkey.

3 | Methods

3.1 | Experimental Design

3.1.1 | Optimization of Experimental Design

A CCD within RSM was employed using Design Expert version 13.0.2.0, software, State-Ease Inc. Minneapolis, MN, USA, to optimize the formulation variables: core-to-coat ratio, incubation time, and drug amount. Analysis of variance (ANOVA) was significant when p < 0.05 and in 95% confidence interval. These factors were evaluated for their effects on particle size, PDI, and zeta potential. The design included 13 experimental runs, allowing for the assessment of linear, interaction, and quadratic effects [16, 18–20].

3.2 | Preparation of AQ

3.2.1 | Preparation of the Core

HAP cores were synthesized via a precipitation method by reacting disodium hydrogen phosphate with calcium chloride under controlled conditions, following established protocols [21]. The equation for the reaction is shown below:

$$2Na_2HPO_4 + 3CaCl_2 + H_2O \rightarrow Ca_3[PO_4]_2 + 4NaCl + 2H_2 + Cl_2 + [O]$$

The resulting precipitate was washed, filtered, and dried to obtain HAP nanoparticles.

3.2.2 | Coating of the Core

HAP cores were coated with various disaccharides (lactose, maltose, sucrose, and trehalose) by dispersing the cores in aqueous sugar solutions, followed by sonication and incubation. The coated cores were then centrifuged, washed, and freeze-dried [21–24].

3.3 | Drug Loading

Curcumin was loaded onto the sugar-coated HAP cores by dissolving it in methanol and mixing it with an aqueous solution of polyvinylpyrrolidone (PVP) and the coated cores. The curcumin:PVP ratio was 1:4 while sugar-coated HAP:curcumin and PVP was 1:1. The mixture underwent homogenization and agitation and was then freeze-dried to obtain curcumin-loaded AQ.

3.4 | Physicochemical Characterization

3.4.1 | Particle Size, PDI, and Zeta Potential Analysis

Particle size, PDI, and zeta potential were measured using a Zetasizer Nano ZS (Malvern Instruments Ltd., UK). Samples were appropriately diluted with distilled water, and measurements were performed at room temperature in triplicate [24, 25].

3.4.2 | Energy-Dispersive X-Ray (EDX) Analysis

Elemental compositions were analyzed using EDX spectroscopy (Hitachi S-3030N, Ireland) to confirm the presence of curcumin and sugars on the HAP core [23].

3.4.3 | Crystallinity

All samples' chemical composition and crystalline structure were obtained through x-ray diffraction powder using a diffractometer with Cu K α radiation at 40 kV/40 mA (RIGAKU, Rotaflex RV 200, Rigaku Corporation, Japan). The scanning rate utilized ranged from 10° to 60° diffraction angle (2 θ) at a speed of 1°/min [22]. The apparatus determines the interlayer spacing, d, derived from the scattering angle θ , using Bragg's equation $n\lambda = 2d\sin\theta$, where λ is the wavelength of the incident x-ray beam, and n is the order of interference. The obtained XRD patterns were compared to assess the intensity of characteristic peaks associated with the drug [26].

3.4.4 | Fourier-Transform Infrared Spectroscopy (FTIR) Analysis

The dried powders of the HAP, coated with cellobiose, lactose, maltose, sucrose, and trehalose, and curcumin-loaded AQ, were prepared for analysis. The instrument Spectrum BX (Perkin Elmer, Massachusetts, USA) was first sterilized and calibrated by reading the blank disk. Then, one at a time, the samples were added by the hydrostatic press at a specific force for a few minutes (2–4). The samples were scanned in the range of 400–4000 cm $^{-1}$ at a resolution of about 4 cm $^{-1}$ [20].

3.4.5 | Differential Scanning Calorimetry (DSC) and Thermogravimetric Analysis (TGA)

Thermal properties were assessed using DSC and TGA with a TA-60WS thermal analyzer (TA Instruments, SDT 650, USA). Samples were heated from 25°C to 800°C at a rate of 10°C/min

under a nitrogen atmosphere to evaluate thermal stability and interactions between components [26].

3.4.6 | Encapsulation Efficiency (EE) and Loading Efficiency (LE)

EE and LE were determined by dissolving known amounts of curcumin-loaded AQ in methanol, centrifuging to separate unloaded drugs, and analyzing the supernatant using UV-vis spectrophotometry at 425 nm. The EE and LE were calculated using the following equations:

$$EE = \frac{Total\ weight\ of\ Cur - Weight\ of\ unloaded\ Cur}{Total\ weight\ of\ Cur} \times 100\%$$

$$LE = \frac{\text{Total weight of Cur} - \text{Weight of unloaded Cur}}{\text{Weight of particles}} \times 100\%$$

3.5 | In Vitro Drug Release Studies

In vitro drug release studies were performed using a USP Type II dissolution apparatus in 0.1 N hydrochloric acid (HCl, pH 1.2) and phosphate-buffered saline (PBS, pH 7.4) at $37 \pm 0.5^{\circ}$ C. Samples were withdrawn at predetermined intervals over 8 h, filtered, and analyzed spectrophotometrically at 425 nm to determine curcumin release [25, 27].

3.6 | In Vitro Release Kinetics

Release data were fitted to various kinetic models, including zero-order, first-order, Higuchi, Korsmeyer-Peppas, and Hixson-Crowell models, to elucidate the drug release mechanisms [28, 29]. Detailed equations are provided in the supplementary material.

3.7 | Stability Studies

3.7.1 | Long Term Stability

Stability studies were conducted at $5 \pm 3^{\circ}$ C and $25 \pm 3^{\circ}$ C over 3 months. Samples were evaluated at 7 days, 14 days, 1-, 2-, and 3-month intervals for total drug content, particle size, PDI, zeta potential, and visual inspection.

3.7.2 | Photostability Studies

Photostability studies were performed according to International Council on Harmonisation (ICH) guidelines. Curcumin-loaded AQ and free curcumin were stored in clear and amber containers and exposed to light (not less than 1.2 million lux hours) for 14 days. Samples were analyzed for total drug content, entrapment efficiency, particle size, zeta potential, and PDI [26].

3.8 | Biocompatibility Evaluation

3.8.1 | Hemolysis Assay

A hemolysis assay was conducted to assess the biocompatibility of curcumin-loaded AQ using rat red blood cells (RBCs). Samples were incubated with RBCs at 37°C, and hemolysis was quantified by measuring absorbance at 540 nm using a microplate reader (BioTek). Triton X-100 and normal saline served as positive and negative controls, respectively. All tests were performed in six replicates [30].

The percentage hemolysis of RBCs was calculated using the following formula:

% Hemolysis

= (Sample Absorbance-Negative Control Absorbance) (Positive Control Absorbance-Negative Control Absorbance) × 100

The results obtained are presented in appropriate graphs

3.9 | Statistical Analysis

Statistical analyses were performed using one-way ANOVA, with p < 0.05 considered statistically significant. Data are presented as mean \pm standard deviation (SD). Visual representations, including box plots, bar charts, and scatter plots, were created using Excel 2019. These visuals facilitated the identification of patterns and outliers in the data.

4 | Results and Discussion

4.1 | Preparation of AQ

The HAP core was synthesized using the precipitation method. It was then coated with sucrose, maltose, trehalose, and lactose sugars. Curcumin was then dissolved in methanol to form the organic phase, while the HAP-coated core and PVP, a hydrophilic carrier, formed the aqueous phase. The solutions were mixed and stirred rapidly to adsorb the drug onto the coated cores. The curcumin-coated AQ were then characterized and studied for in vitro stability, drug release, and permeability.

4.2 | Optimization of Formulation

Table 1 shows the optimization process. This study utilized a CCD to systematically evaluate the effects of the core-to-coat ratio (A), incubation time (B), and drug amount (C) on the particle size, PDI, and zeta potential of the AQ. Statistical analysis using ANOVA indicated that all factors significantly influenced the responses (p < 0.05). The optimal formulation (Run 8) was identified based on the highest desirability factor (0.8385), balancing all responses within the desired range. This formulation had a core-to-coat ratio of 3:1, an incubation time of 6.5 h, and a drug amount of 300 mg, resulting in a particle size of 333.7 nm, a PDI of 0.497, and a zeta potential of -23.9 mV.

4.2.1 | Influence of Factors

A higher core:coat ratio correlates with less negative zeta potential, which might indicate less stability. However, this factor does not show a consistent particle size or PDI trend. Longer incubation times yield a more negative zeta potential and smaller particle sizes. Higher drug amounts tend to decrease the zeta potential, suggesting a less stable colloidal system. This factor also shows no consistent trend with particle size or PDI. To optimize for stability and uniformity, focusing on the appropriate incubation time and adjusting the core:coat ratio may be more influential than altering the amount of the drug. All the factors were statistically significant, as shown in the tables below, and their equations in 2FI and quadratic models are shown in Figures 1–4.

Quality is an essential factor in the development of pharmaceutical products, serving as the primary focus for regulatory bodies to ensure the approval of drug delivery systems that are safe, effective, stable, patient-friendly, and cost-effective. Within this framework, the QbD approach for formulation development is increasingly becoming central to the operations of pharmaceutical companies. This computational strategy has been utilized extensively to develop a variety of vesicular nanocarriers, including liposomes, niosomes, transferosomes, AQ, and polymeric micelles. This study explored the CCD technique to optimize the AQ formulations [32].

Zeta potential =
$$-33.7893 + 2.95916 * A + 1.59776 * B$$

+ $0.0158844 * C + -0.0798864 * AB$
+ $0.000696875 * AC + -0.0038125 * BC$

The ANOVA analysis for zeta potential revealed that the model was significant (F value = 5.16, p = 0.0330), indicating a reliable prediction of the experimental data. Among the factors, the core-to-coat ratio (A) (p = 0.0047) and the interaction between incubation time and drug amount (BC) (p = 0.0238) had significant effects on the zeta potential. Specifically, increasing the core-to-coat ratio resulted in less negative zeta potential values, suggesting a potential decrease in colloidal stability. The non-significant lack of fit (p = 0.8454) confirmed the adequacy of the model.

Particle Size =
$$57.7544 + 56.9901 * A + 36.0751 * B$$

+ $0.183089 * C + -6.97159 * AB$
+ $0.111844 * AC + -0.0867159 * BC$

For particle size, the model was highly significant (F value = 12.04, p = 0.0040), with the core-to-coat ratio (A) (p = 0.0028), incubation time (B) (p = 0.0184), and their interactions (AB and BC) (p = 0.0116 and p = 0.0043, respectively) showing significant influence. The results indicated that both higher core-to-coat ratios and longer incubation times led to increased particle sizes (Figure 2). The interactions between factors emphasized the complexity of the formulation process, where simultaneous optimization of variables is necessary. The lack of

FIGURE 1 | Effect of incubation time and core:coat ratio on zeta potential (mV).

Factor Coding: Actual

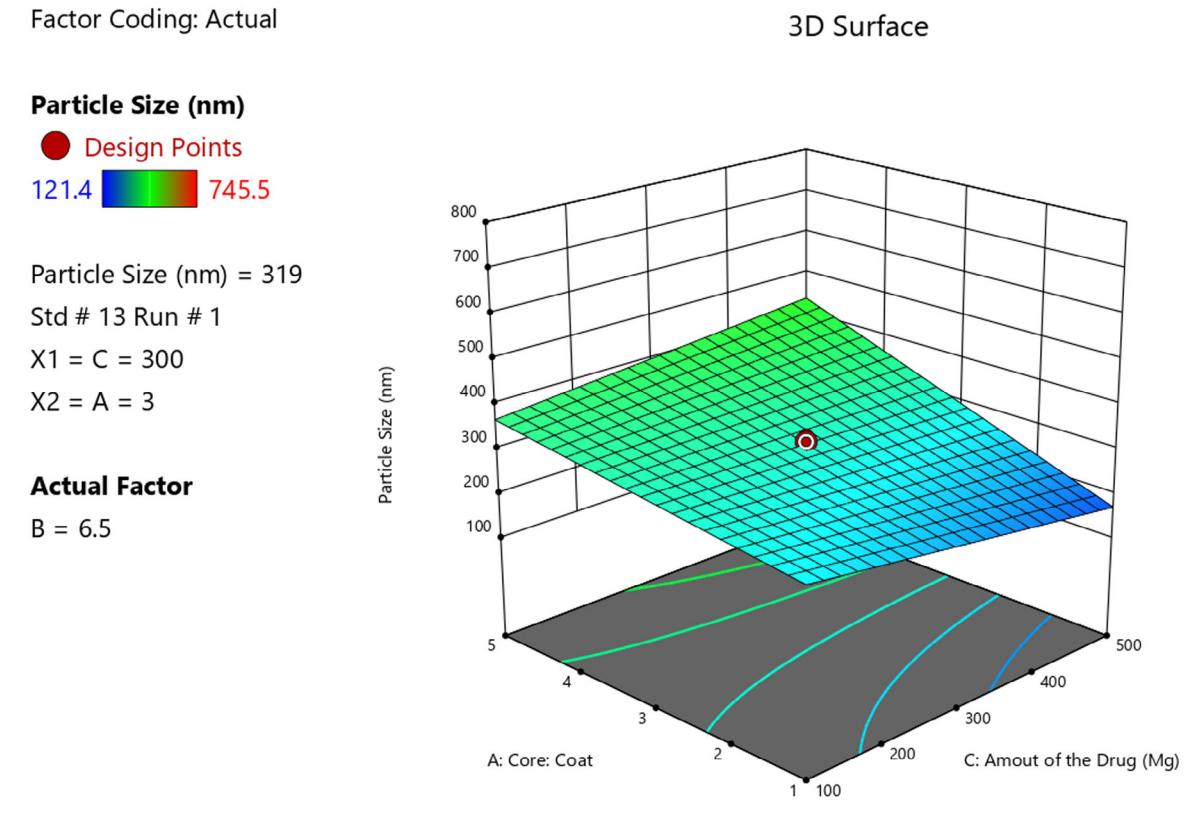


FIGURE 2 | Effect of core:coat and amount of the drug on particle size (nm).

and-conditions) on Wiley Online Library for rules of use; OA articles are governed by the applicable Creative Commons License

26884011, 0, Downloaded from https://onlinelibrary.wiley.com/doi/10.1002/nano.202400162 by Nat Prov Indonesia, Wiley Online Library on [13.01/2025]. See the Terms and Conditions (https://onlinelibrary.wiley.com/term

3D Surface

Polydispersity Index

Design Points:

Above Surface

Below Surface

0.254 0.813

Polydispersity Index = 0.575

Std # 13 Run # 1

X1 = A = 3

X2 = B = 6.5

Actual Factor

C = 300

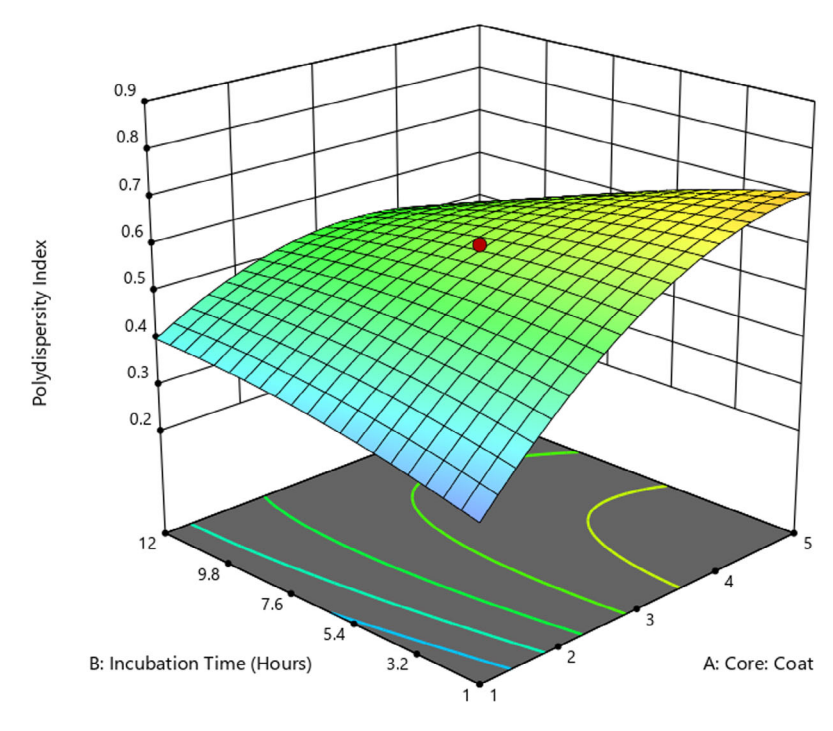


FIGURE 3 | Effect of incubation time and core:coat on PDI.

Factor Coding: Actual

3D Surface

Desirability

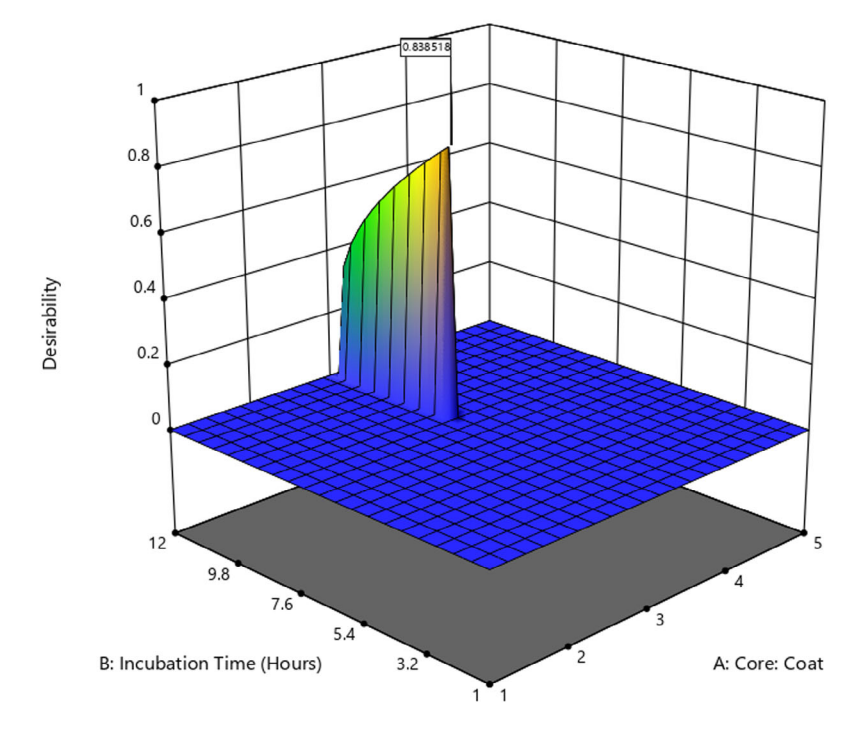


X1 = A

X2 = B

Actual Factor

C = 354.791



 $\textbf{FIGURE 4} \hspace{0.1in} \mid \hspace{0.1in} \textbf{Effect of incubation time and core:} coat on desirability.$

TABLE 1 Experimental results concerning the tested variables on the mean particle size of AQ.

	Factor 1	Factor 2	Factor 3	Response 1	Response 2	Response 3
Run	A: Core:Coat	B: Incubation time Hours	C: Amount of the drug	Zeta potential mV	Particle size	Polydispersity index
1	3	6.5	300	-15.7 ± 4.1	319.0 ± 10.3	0.575 ± 0.210
2	1	1	500	-21.8 ± 1.2	224.0 ± 16.4	0.391 ± 0.171
3	1	12	500	-24.2 ± 3.4	121.4 ± 15.8	0.298 ± 0.243
4	1	1	100	-26.9 ± 2.4	191.7 ± 12.8	0.254 ± 0.180
5	6.4	6.5	300	-9.1 ± 2.7	407.5 ± 20.5	0.536 ± 1.131
6	3	6.5	636.4	-25.6 ± 0.8	248.1 ± 11.4	0.675 ± 0.282
7	5	12	500	-17.0 ± 4.6	191.7 ± 20.6	0.381 ± 0.130
8	3	6.5	300	-23.9 ± 1.7	333.7 ± 9.7	$\boldsymbol{0.497 \pm 0.262}$
9	5	1	500	-6.71 ± 3.9	745.5 ± 13.2	0.813 ± 0.094
10	5	1	100	-17.3 ± 2.7	389.8 ± 19.4	0.648 ± 1.016
11	3	15.7	300	-15.4 ± 5.3	257.0 ± 15.9	0.497 ± 0.635
12	1	12	100	-16.9 ± 4.7	326.2 ± 16.3	0.541 ± 1.314
13	5	12	100	-6.4 ± 5.6	362.0 ± 22.8	0.573 ± 0.806

fit was non-significant (p = 0.1188), validating the model's fit.

PDI =
$$-0.0247661 + 0.254149 * A + 0.0526414 * B + 4.09216e$$

 $-06 * C + -0.00796591 * AB + 2.46875e - 05 * AC +$
 $-8.375e - 05 * BC + -0.0248219 * A2$
 $+-0.00075001 * B^2 + 6.83259e - 07 * C2$

The quadratic model for PDI was also significant (F value = 25.95, p=0.0108). Significant factors included the core-to-coat ratio (A) (p=0.0021), the interactions between core-to-coat ratio and incubation time (AB) (p=0.0060), incubation time and drug amount (BC) (p=0.0052), and the quadratic term of the core-to-coat ratio (A²) (p=0.0068). These findings suggest that higher core-to-coat ratios and specific interactions between variables increase PDI, indicating a broader particle size distribution (Figure 3). The non-significant lack of fit (p=0.3231) further supported the model's suitability. For details on the ANOVA tables, refer to the supporting information, Tables S1–S3.

The desirability is a function that likely represents the optimal conditions for a process or reaction to maximize this value. The plot shows that the peak desirability is bright green and occurs at a specific region in the factor space (Figure 4). The "Actual Factor" C is given as 354.791, which might represent a fixed condition or parameter that is not varied in the experiment. The highest desirability, indicated at the top of the peak, is 0.838518, suggesting a favorable outcome under these specific conditions. The "Core: Coat" ratio at which peak desirability occurs is closer to the lower end of the scale (which is shown as "1" on the axis), suggesting a lower ratio is more desirable. The "Incubation Time" corresponding to the peak desirability seems to be on the lower end of the provided time range. AQ were synthesized under optimized conditions to assess the predictive accuracy of

the model and its desirability coefficient. The experimental values obtained for AQ prepared using these optimal conditions closely matched the predicted values, exhibiting minimal percentage bias

A previous study by Kaur et al. achieved a maximum desirability coefficient (d) of 0.701 under specific conditions (core:coat ratio of 1:3, sonication power of 12.5 W, and sonication time of about 55 min) [20]. In contrast, this study had a higher peak desirability of 0.838518. The optimum sonication time and power were adopted for this study, which could be one of the factors to explain the differences [21]. Both studies indicate the importance of the core:coat ratio in achieving optimal desirability and found that a lower ratio is more desirable. Both studies highlight the predictive power of the model used to determine desirability. The close match between predicted and experimental values in this study, with minimal percentage bias, confirms the model's accuracy. However, the differences in optimal conditions and desirability values suggest that the model may be sensitive to each study's specific parameters and conditions.

HAP is widely recognized as a stable, cost-efficient, and biodegradable substrate for scaling drug delivery systems [33]. Its compatibility with a broad spectrum of therapeutic agents, ranging from low to high molecular weights, makes it a versatile medium for drug carriage. In terms of thermodynamic stability, HAP stands out as the most stable form of calcium phosphate under physiological conditions, including pH, temperature, and fluid composition, endorsing its suitability for biomedical applications [34].

PVP is a water-soluble polymer that offers several advantages when used in aquasome delivery systems for curcumin. PVP enhances the solubility of hydrophobic molecules like curcumin, thus increasing its bioavailability [27]. Additionally,

TABLE 2 | Analysis of particle size, PDI, and zeta potential of core, coated core with sugars, and curcumin-loaded AQ with PVP.

Formulation	Zeta potential (mV) Mean ± SD	Particle size (nm) Mean ± SD	PDI Mean ± SD
HAP	-35.1 ± 1.42	55.41 ± 6.4	0.374 ± 1.01
Lactose-coated HAP	-25.4 ± 2.8	149.6 ± 9.1	0.503 ± 0.60
Sucrose-coated HAP	-27.8 ± 2.22	136.6 ± 13.5	0.555 ± 0.58
Trehalose-coated HAP	-24.2 ± 0.87	138.1 ± 5.8	0.530 ± 1.74
Maltose-coated HAP	-27.4 ± 2.40	180.7 ± 6.7	0.565 ± 0.84
Curcumin-loaded AQ-lactose	-23.9 ± 1.7	333.7 ± 9.7	0.497 ± 0.262
Curcumin-loaded AQ-sucrose	-21.1 ± 3.44	215.6 ± 12.4	0.601 ± 0.83
Curcumin-loaded AQ-trehalose	-22.9 ± 2.88	255.1 ± 22.1	0.421 ± 1.68
Curcumin-loaded AQ-maltose	-20.9 ± 3.61	329.5 ± 17.5	0.473 ± 0.94

PVP stabilizes curcumin against degradation by providing a protective colloid environment, which is crucial given curcumin's sensitivity to light and oxygen [1]. Furthermore, PVP's role as a steric stabilizer helped prevent the aggregation of AQ, ensuring a consistent and controlled release profile [35]. The biocompatibility of PVP also minimizes potential cytotoxicity, which is a significant concern in developing drug delivery systems [36]. Therefore, utilizing PVP in AQ not only improves the therapeutic efficacy of curcumin but also broadens the scope of conditions that curcumin can potentially treat due to solubility and stability [37].

4.3 | Physicochemical Characterization

4.3.1 | Particle Size, Zeta Potential, and PDI

Table 2 shows the particle size, PDI, and zeta potential of the core, the coated core with sugars, and curcumin-loaded AQ with PVP. HAP has the highest negative zeta potential (-35.1 mV), indicative of a stable colloidal system due to repulsion between particles, minimizing aggregation risk. The coated HAP formulations have lower negative zeta potentials than uncoated HAP, suggesting that the coating process may reduce surface charge and, thus, colloidal stability. However, they are still likely to be relatively stable as they are beyond -20 mV. Curcumin-loaded AQ show significantly lower negative zeta potentials, especially when compared to pure HAP. This suggests that curcumin and the sugar coatings may interact with the surface to reduce the overall charge, which might affect the stability.

The pure HAP shows the smallest particle size (55.41 nm), often desirable for drug delivery applications due to better tissue penetration and distribution. The coating with sugars increases the particle size. The curcumin-loaded AQ formulations show increased particle size compared to pure HAP, which is expected due to the additional molecular layers. The smallest particle size in this group is seen with sucrose coating, which may indicate better packing efficiency or interaction with curcumin.

HAP has a PDI of 0.374, indicating a relatively narrow size distribution, which is generally preferred as it predicts a more uniform behavior in biological systems. All coated and curcumin-

loaded formulations have higher PDI, indicating broader size distributions. While this can be acceptable, it may lead to more variable drug release rates and biological interactions. Curcuminloaded AQ formulations generally have higher PDI than pure and coated HAP, with sucrose showing the highest PDI (0.601). This could be due to aggregation or a more diverse particle size. The increase in particle size and PDI with sugar coatings and curcumin loading suggests that the coating and drug loading process significantly alters the physical characteristics of the particles.

A change in particle size and zeta potential was observed with the coating of the sugars and adsorption of the drug. Similarly, previous studies had followed this trend [20, 21, 23]. The coating process introduces a new surface layer, which can shield the original core charge and increase the hydrodynamic radius. The adsorption of curcumin onto the coated cores further modifies the zeta potential, reducing it due to the partial neutralization of surface charges by the hydroxyl, keto and methyl groups. The particle size also increases due to the additional layer formed by the adsorbed Curcumin.

4.3.2 | EDX Analysis

The EDX analysis (Figure 5) shows the elemental composition of HAP, sugar-coated HAP, and curcumin-loaded AQ. The elemental composition shows a high percentage of calcium (Ca) and oxygen (O), with phosphorus (P) also present, which are the primary components of HAP. The weight and atomic percentages suggest a stoichiometry that may be consistent with pure HAP.

Lactose-coated HAP EDX Analysis showed the presence of carbon (C) which indicates the incorporation of lactose. The ratio of Ca to P seems slightly altered compared to pure HAP, likely due to the addition of lactose. The oxygen content also differs, reflecting the chemical changes due to lactose loading.

Curcumin-loaded AQ EDX analysis shows C, O, P, and Ca, and the N from PVP. The Ca to P ratio is essential for the bioactivity of HAP, and the loading with curcumin may have altered this ratio slightly. The EDX data suggests successful loading of curcumin onto the HAP.

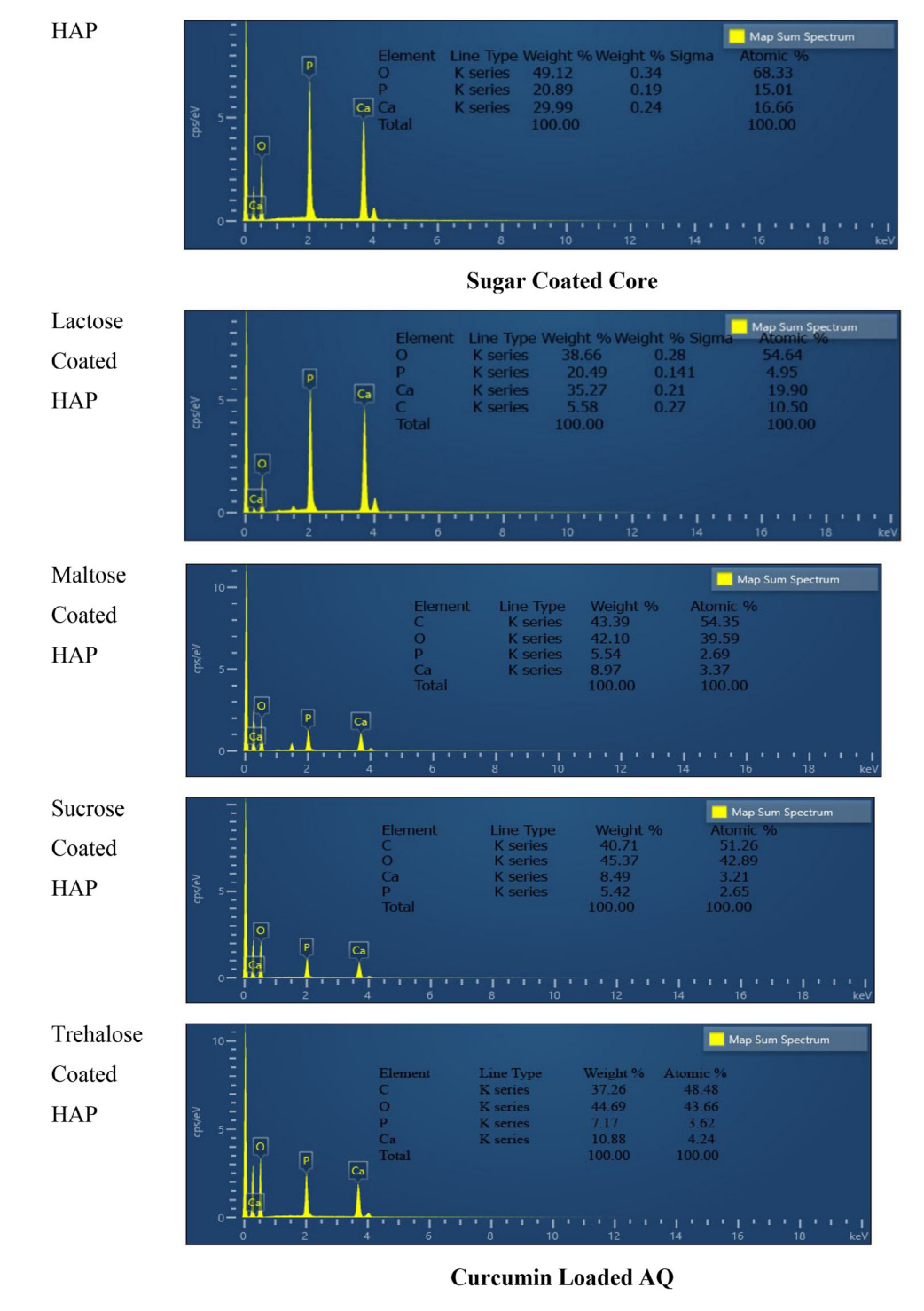


FIGURE 5 | EDX analyses of HAP, sugar-coated core, and curcumin-loaded AQ.

The Ca/P ratio across the samples, though slightly altered, is consistent. It affects the crystallinity and stability of HAP, which in turn influences drug delivery properties. Therefore, the HAP is providing stability to the drug in the aquasome drug delivery system.

4.3.3 | EE and LE

Different formulations of curcumin were evaluated for their encapsulation and loading efficiencies as shown in Table 3. The

encapsulation efficiency refers to the ability of the formulation to retain the encapsulated compound. In contrast, the loading efficiency represents the amount of the compound loaded into the formulation relative to the total amount used during the encapsulation process.

Based on the results obtained, it is evident that the curcuminloaded AQ-trehalose formulation exhibited the highest encapsulation efficiency of 55.1%. This indicates a successful encapsulation process that effectively retained the curcumin within the formulation. Furthermore, % loading efficiency of 35.3% suggests

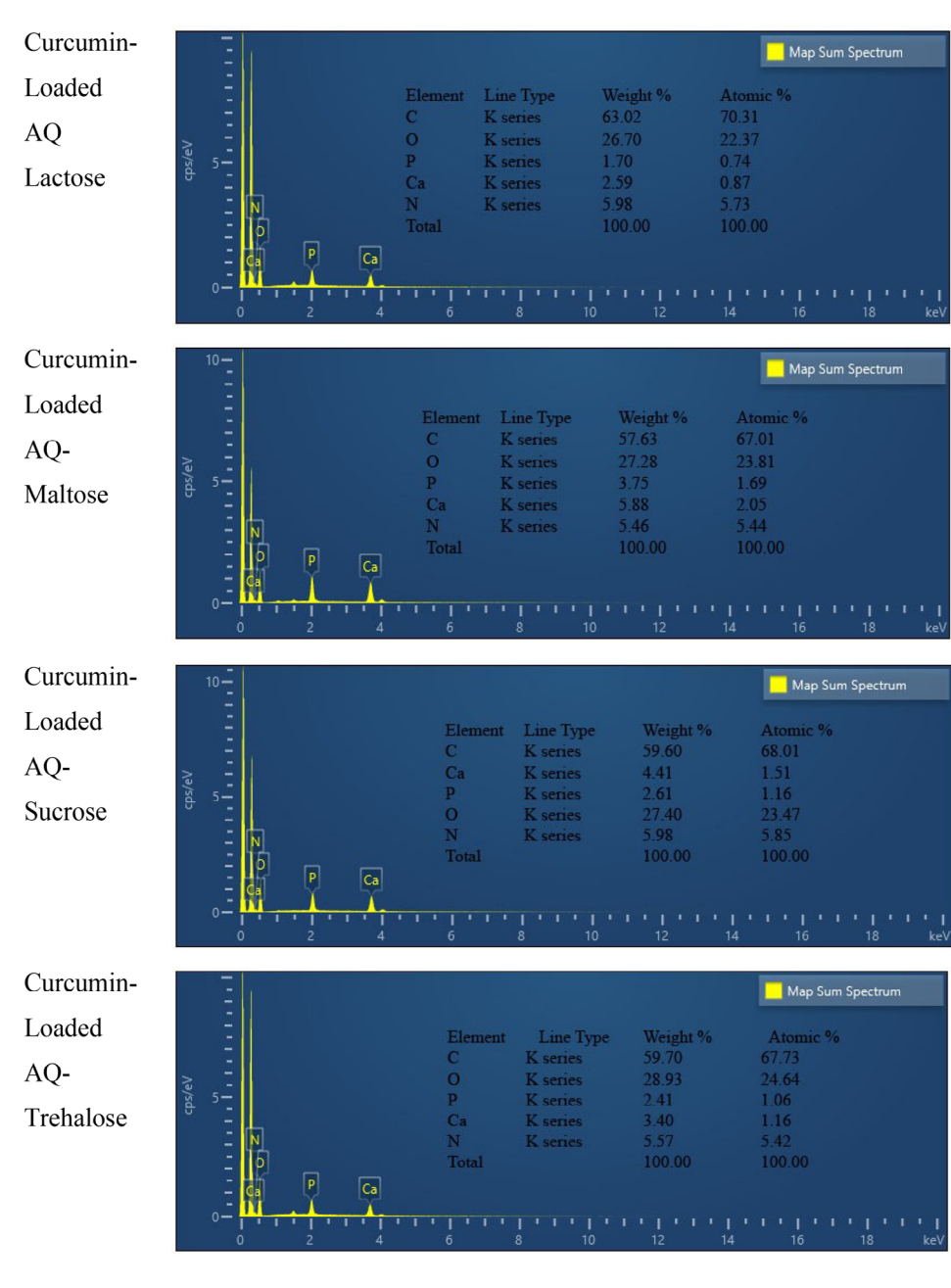


FIGURE 5 | (Continued)

TABLE 3 | Measurement of encapsulation efficiency (%) and loading capacity (%).

Formulation	Encapsulation efficiency (%)	Loading efficiency (%)
Curcumin-loaded AQ-lactose	53.67 ± 0.48	32.2 ± 0.55
Curcumin-loaded AQ-sucrose	$52.0 \pm 0.0.36$	31.2 ± 0.83
Curcumin-loaded AQ-trehalose	55.1 ± 0.21	35.3 ± 0.64
Curcumin-loaded AQ-maltose	50.0 ± 0.92	30.0 ± 0.74

that a substantial amount of curcumin was successfully loaded into the AQ-trehalose formulation.

Similarly, the curcumin-loaded AQ-sucrose formulation demonstrated a relatively high encapsulation efficiency of 52.0%.

This suggests a successful encapsulation process with effective retention of curcumin within the AQ-sucrose formulation. Additionally, a loading efficiency of 31.2% indicates a considerable amount of curcumin being successfully loaded into the formulation.

The curcumin-loaded AQ-maltose formulation exhibited a slightly lower encapsulation efficiency of 50% and a loading efficiency of 30%. Although still reasonably efficient, these results indicate a relatively lower retention of curcumin within the AQ-maltose formulation compared to the other two formulations.

The higher encapsulation and loading efficiencies observed in the curcumin-loaded AQ-lactose and AQ-trehalose formulations suggest that they could be promising candidates for further investigation regarding their potential applications in drug delivery systems or functional food formulations.

The encapsulation efficiencies from this study ranged from 50% to 55.1%, a carbohydrate carrier (lactose, sucrose, trehalose, and maltose). These findings are significantly higher than those reported in Vengala's study, where the drug loading was found to be only 8.53% [21]. This difference can be attributed to the optimization of aquasome formulations in the current study by selecting carriers or excipients that enhance drug loading efficiency. Similarly, the findings surpass the maximum drug loading efficiency reported by Kommineni et al., $23.32\% \pm 0.886\%$ [38]. The improved performance in my study might be due to the functionalization of AQ with the polymer PVP, which can enhance drug adsorption and solubility [37]. The CLEN study and the research on voriconazole-loaded AQ for the treatment of fungal infections reported entrapment efficiencies significantly higher than those observed in this study, with values of $79.74\% \pm 0.88\%$ and 81.74%, respectively [26, 28]. Additionally, Yin's study reported an even higher yield of 91.59% \pm 4.49% and encapsulation efficiency of 99.93% \pm 0.01% for CURN [27]. These higher efficiencies could be attributed to the differences in the nanoparticles used, their surface chemistry, or the methodologies applied for encapsulation and entrapment.

4.3.4 | XRD

The XRD analysis images (Figure 6) provide insight into the structural properties of HAP, sugar-coated HAP, and curcumin-loaded AQ. The XRD patterns of HAP show prominent peaks at a 2θ around 30°, indicating a crystalline structure. Upon coating with different sugars—lactose, maltose, sucrose, and trehalose—the XRD patterns show additional peaks or broadening of the original peaks, suggesting successful coating and potential changes in crystallinity.

When curcumin is loaded onto the sugar-coated HAP, the XRD patterns reveal a significant reduction in peak intensity and broadening, particularly noticeable in the lactose- and maltose-coated formulations. This change indicates a potential amorphization of curcumin, enhanced dispersion within the carrier, or a possible interaction between curcumin and the sugar-coated HAP, leading to altered crystalline characteristics. The comparison of pure curcumin's XRD pattern with the loaded formulations further supports these observations, as pure curcumin exhibits distinct peaks that are less prominent or absent in the loaded samples.

In this study, prominent crystalline peaks at around $2\theta = 30^{\circ}$, characteristic of the HAP core, were observed, aligning with the

findings of Damera et al., who reported similar peaks at $2\theta = 31^{\circ}$ and 32° [30, 39]. This alignment suggests that the basic crystalline structure of HAP was maintained, even after coating with sugars lactose, maltose, sucrose, and trehalose. However, as noted by Damera et al., a decrease in the intensity of these peaks was observed after coating, indicating a reduction in crystallinity due to the amorphous nature of the coating materials disrupting the crystalline structure of HAP [30].

When comparing these results with those of Kaur et al., it was observed that the reduction in peak intensity and transformation towards an amorphous structure in the curcumin-loaded AQ parallels the findings in their study, particularly in the context of the maximal amorphization observed in Py-5-P-Aq.somes [20]. This similarity may be attributed to the hydrophilic nature of the coating sugars, which, like the polyhydroxy oligomers in Kaur's study, promote hydrogen bonding and consequently reduce crystallinity.

A decrease in crystalline peaks was also observed by Thakare et al. when cellobiose was coated on gelatin cores [40]. However, in this study, no new peaks corresponding to the coating materials were detected, which could suggest that the crystallinity was more effectively suppressed or that the coating was more homogenous.

Rojas-Oviedo highlighted that the transition to an amorphous state is common during processes like lyophilization, which can disrupt the crystalline structure. Similar amorphous characteristics were observed in this study, especially with lactose-coated samples, consistent with Rojas-Oviedo's findings [22]. This suggests that the method of coating and subsequent drying likely plays a significant role in the observed amorphous transition.

Goyal et al. provided evidence of the crystalline nature of HAP with strong peaks around $2\theta = 31^{\circ}-32^{\circ}$, which is corroborated by this study [34]. The persistence of these peaks in the uncoated HAP samples further validates the crystalline nature of the core material before the application of any coatings.

4.3.5 | FTIR

Based on the characteristic bands observed (Figure 7 and Table 4), the final formulations can confirm the presence of HAP, lactose, maltose, trehalose, sucrose, curcumin, and PVP.

From the FTIR analysis of pure curcumin and curcumin-loaded AQ, it was observed that the structure of the pure curcumin and curcumin-loaded AQ was slightly different. Also, the sugarscoated HAP (lactose, sucrose, maltose, and trehalose) slightly differed from the free HAP. Therefore, the FTIR analysis confirmed the formation of AQ through intermolecular hydrogen bonding by broadening shifting peaks at either higher or lower wavelengths.

The FTIR analysis highlights intermolecular interactions critical to the delivery system's stability and function. The shifts and broadening in specific peaks point towards forming hydrogen bonds, which are vital in encapsulation. These interactions

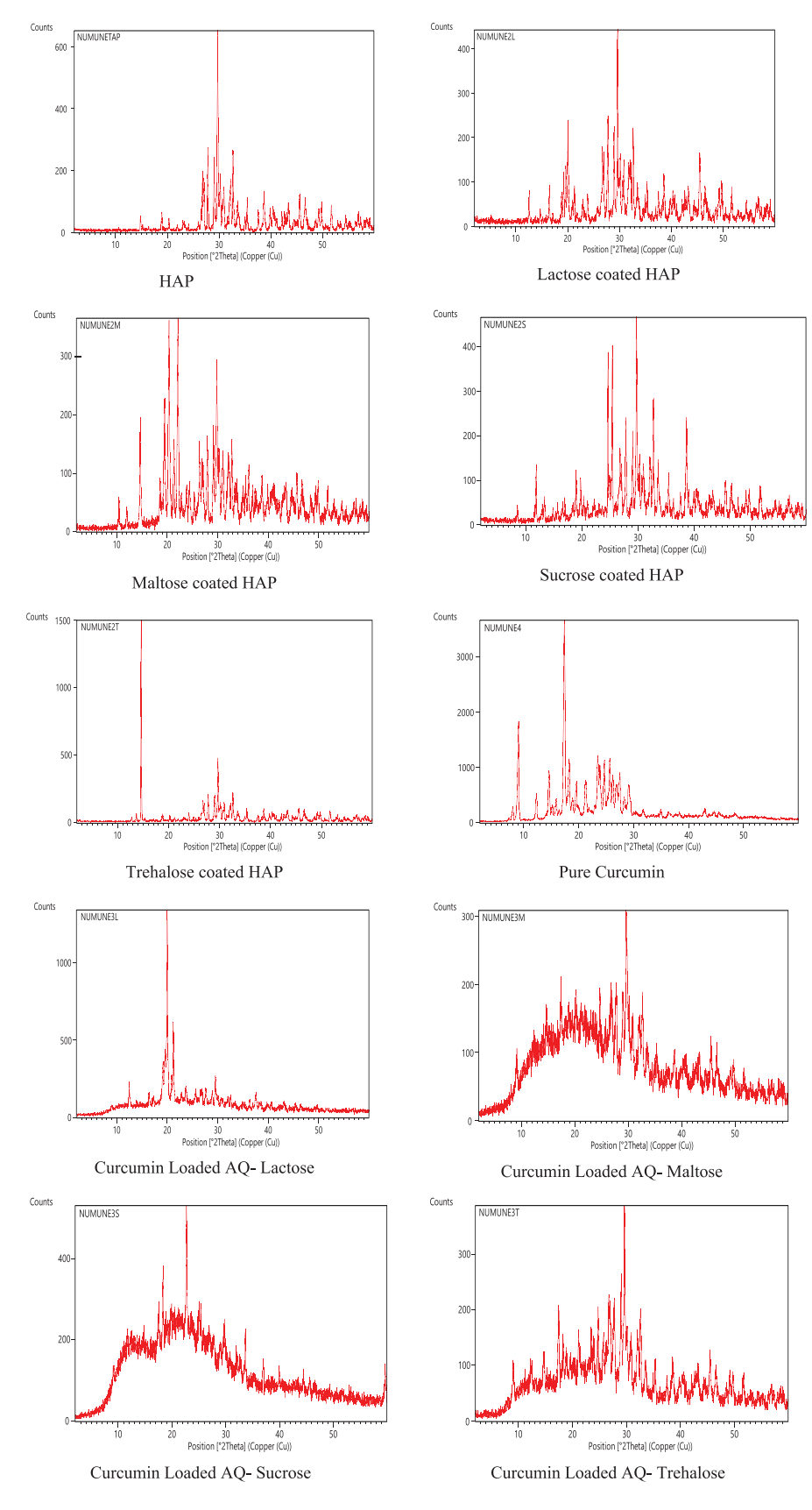


FIGURE 6 | XRD patterns of HAP, sugar-coated HAP, and curcumin-loaded AQs.

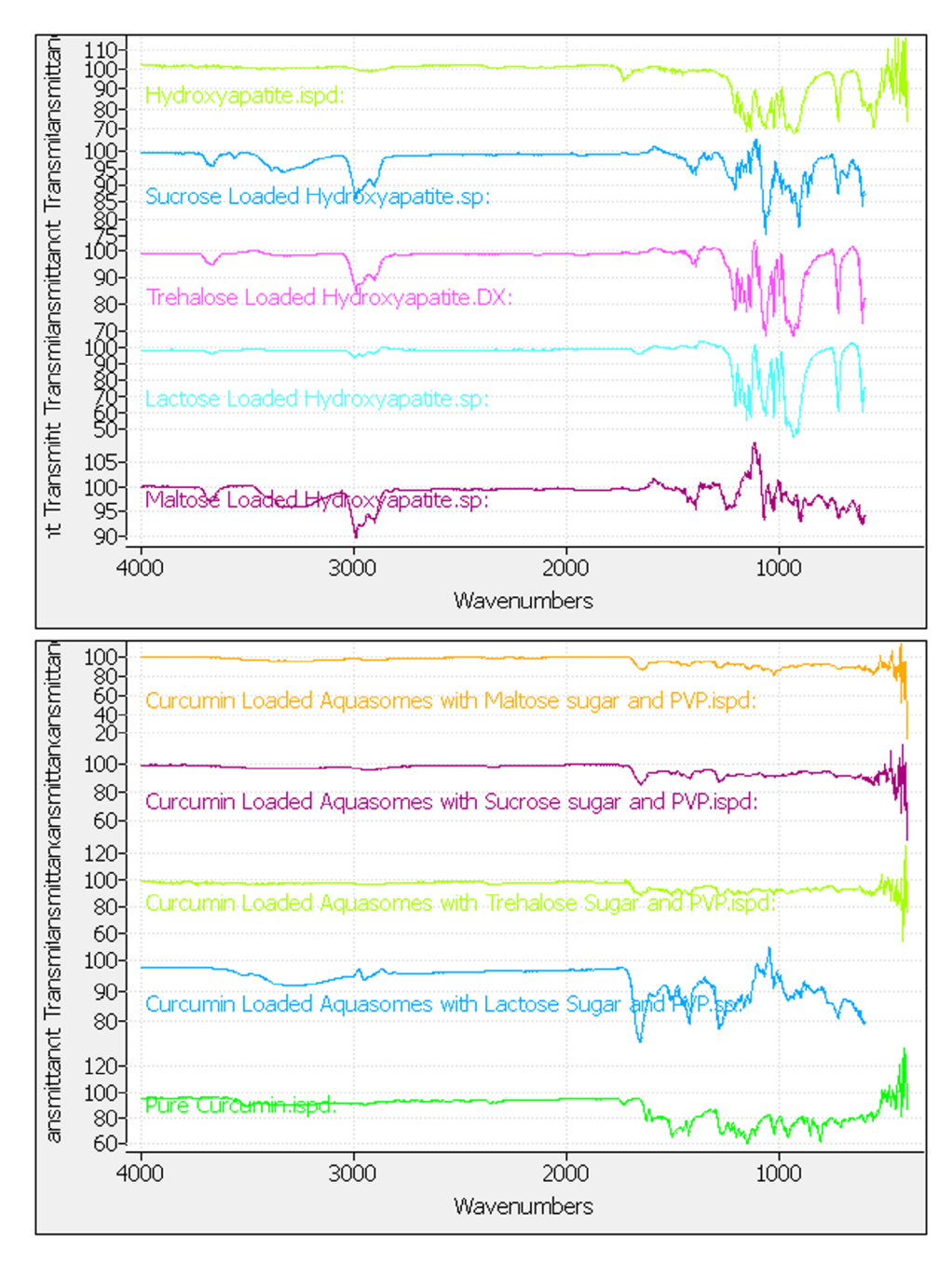


FIGURE 7 | FTIR of HAP, sugar-coated core, and curcumin-loaded AQ.

confirm the encapsulation of curcumin and suggest a level of structural organization within the aquasome that may contribute to its functional properties, such as enhanced solubility and stability. Moreover, the interaction between curcumin and the sugar coatings, as evidenced by shifts in the FTIR spectra, could play a crucial role in protecting the curcumin from degradation and enhancing its bioavailability.

4.3.6 | TGA and DSC

The TGA results (Figure 8) provide insight into the thermal stability and composition of various curcumin-loaded AQ, coated with different disaccharides. The TGA graph for pure HAP shows its inherent thermal stability, with weight loss (less than 1%)

typically due to the removal of physically adsorbed water and decomposition of any surface impurities. The TGA curve for lactose-coated HAP shows additional weight loss stages (15%) compared to pure HAP, indicating the presence of lactose. The thermal decomposition of lactose exhibits weight loss at 200–250°C, corresponding to the melting and decomposition of lactose. Similar to lactose-coated HAP, the maltose-coated HAP TGA curve exhibits weight loss (50%) at 100–450°C, associated with the thermal decomposition of maltose. The sucrose-coated HAP shows characteristic weight loss (50%) due to the decomposition of sucrose at 150–420°C. The TGA curve for trehalose-coated HAP shows weight loss (30%) at 200–380°C, indicating the presence and thermal behavior of trehalose on HAP. Each disaccharide decomposes at a specific temperature, and this decomposition is reflected in the weight loss stages of the TGA curves.

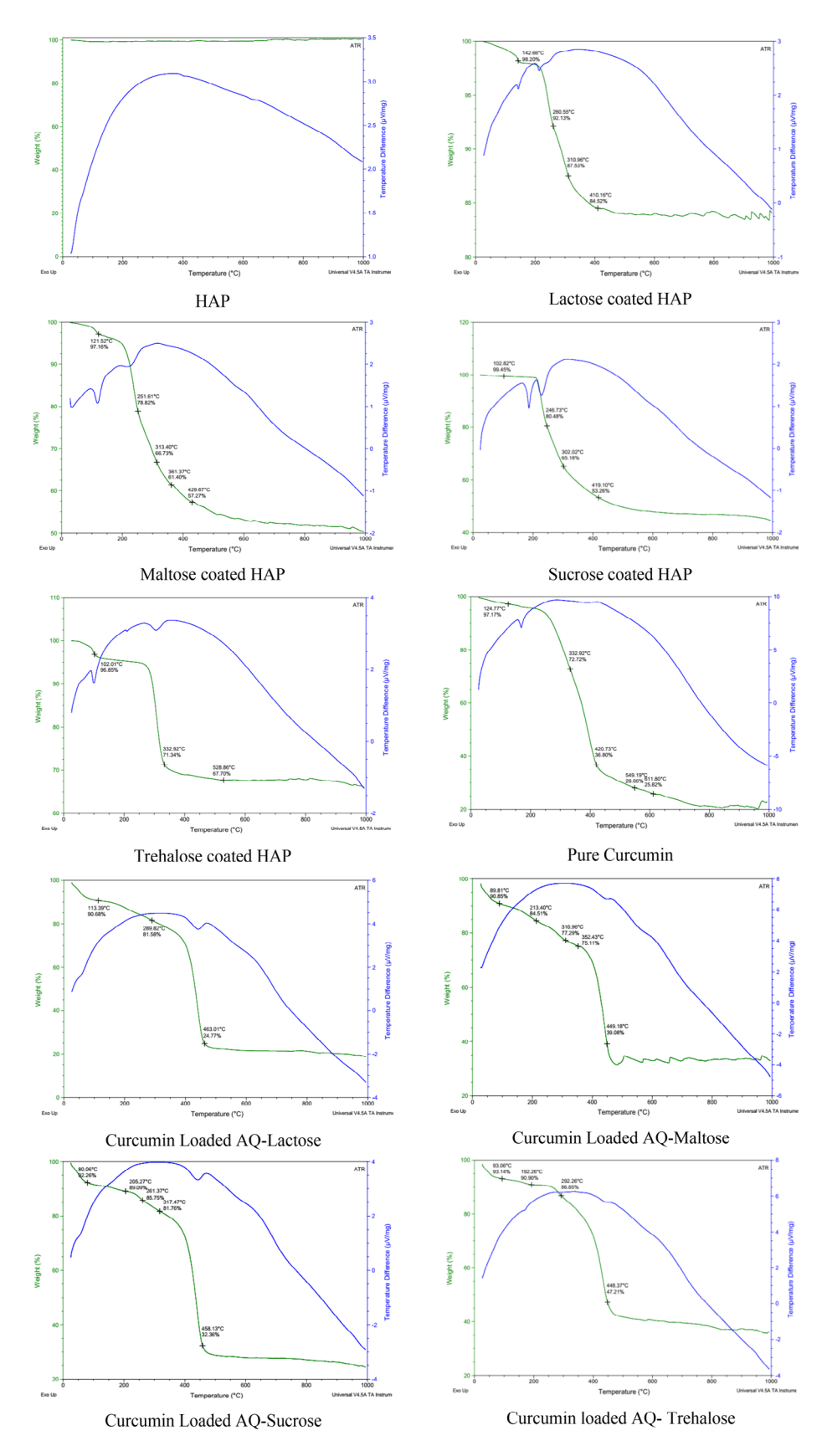


FIGURE 8 | TGA and DSC graphs.

TABLE 4 | Comparison of characteristic IR bands in HAP, sugar-coated core, and curcumin-loaded AQ.

Characteristic bands	Observed in this study, (cm ⁻¹)	Literature values (cm ⁻¹)
Core		
Phosphate (P—O)	725.79	725–845 [41]
Phosphate $(P = O)$	1066, 1210	1240–1300 [42]
Lactose/Maltose/Sucrose/Trehalose		
CH ₂ stretching	2901.2–2990	2800–3000 [21, 43]
Carbonyl $(C = O)$	1658.1	1750 [21, 38]
ОН	1410.02, 3663.3	1400–1600, 3200–3600 [21]
C—O—C linkages	1000–1215	1000 and 1300 [21, 38]
C—O stretching	1000–1215	1000–1300 [21, 38]
Curcumin		
ОН	3200–3530	3200–3600 [25]
C = O	1647–1660	1700–1750 [44]
C = C	1600–1605	1600–1605 [25, 26]
С—Н	2950-3100	3000-3100 [44]
C—O stretch	1000-1300	1000–1300 [25, 26]
Polyvinylpyrrolidone		
C = O	1647–1660	1650–1680 [35]
C-N	1500–1560	1530–1560 [36]
С—Н	2800–3000	2800–3000 [35, 36]
C-O	1100–1250	1100–1250 [35, 36]

The TGA graph for pure curcumin shows its thermal degradation pattern, highlighting the temperatures (175-700°C) at which curcumin decomposes. The TGA curve for curcumin-loaded AQ-lactose shows the combined thermal degradation patterns of both lactose and curcumin, with weight loss (80%) indicating the loss of lactose and the decomposition of curcumin at 300-425°C. Similarly, the TGA curve for curcumin-loaded AQsucrose shows the combined thermal behaviors of sucrose and curcumin at 300-425°C with 70% weight loss. The TGA graph for curcumin-loaded AQ-trehalose shows weight loss (60%) due to the decomposition of trehalose and curcumin at 200-425°C. The TGA curve for curcumin-loaded AQ-maltose shows weight loss (70%) at the decomposition temperatures of 200-450°C of both maltose and curcumin. The differences in weight loss between curcumin and the curcumin-loaded AQ can be attributed to the presence and decomposition of the coating disaccharides and the PVP hydrophilic carrier. The TGA for the pure curcumin obtained in this study is similar to that in a similar study by Jafari et al. [45].

The TGA results from this study were compared to those reported by Damera et al. [30], revealing both similarities and differences. Both studies observed minimal weight loss in HAP, with this study showing less than 1% weight loss due to the removal of physically adsorbed water and surface impurities, while Damera et al. reported about 4% weight loss, attributed to the loss of physically adsorbed and chemically bound water. The influence of coating materials on TGA curves was evident in both studies; for instance, lactose-coated HAP in this study exhibited a 15% weight

loss, whereas cellobiose-coated HAP in Damera et al.'s study showed about 10% weight loss at similar temperature ranges, confirming the decomposition of coating materials. Differences were observed in the weight loss percentages and decomposition temperature ranges. Lactose in this study decomposed at 200-250°C, while cellobiose in Damera et al.'s study decomposed at around 250°C, indicating slight variations due to the different disaccharides used. Furthermore, this study included various disaccharide-coated HAP samples (lactose, maltose, sucrose, trehalose), each showing distinct weight loss percentages and temperature ranges, whereas Damera et al. focused on cellobiosecoated HAP and AQ/BSA, showing about 20% weight loss due to BSA decomposition at 45°C and 400-500°C [30]. These differences can be attributed to the specific thermal properties of the coatings used and the broader range of samples analyzed in this study.

The DSC curve (Figure 8) of HAP alone presented a baseline with no significant transitions, indicating its stability up to the studied temperatures. There is an exothermic peak of up to 400°C due to the crystallization of HAP. Lactose-coated HAP showed endothermic peaks at 142.66°C and 220°C due to the melting and decomposition of lactose. Maltose-coated HAP showed endothermic peaks at 121.52°C and 240°C and a mild exothermic peak around 300°C. The endothermic peaks correspond to the melting and subsequent degradation of maltose. Sucrose-coated HAP showed endothermic peaks at 200°C and 220°C, with a mild exothermic peak around 302°C. This corresponds to the melting of sucrose, followed by its decomposition at higher temperatures.

Trehalose-coated HAP showed endothermic peaks at 102.01°C, 205°C, and 309°C, indicating the melting and degradation of trehalose.

Pure curcumin exhibited endothermic peaks at 181°C, associated with the melting point of curcumin, and further degradation around 400°C. For the curcumin-loaded AQ, the DSC curves revealed complex thermal behavior due to the interaction between curcumin, the PVP carrier, and the carbohydrate coatings. Curcumin-loaded AQ prepared with lactose-coated HAP showed an endothermic peak at 447°C. The peaks are due to the melting of lactose, PVP, and curcumin, followed by the degradation of curcumin. Curcumin-loaded AQ prepared with maltose-coated HAP showed a mild endothermic peak of 448°C. The endothermic peak suggests the melting of maltose, while the later peaks correspond to the decomposition of the maltose, curcumin, and PVP. Curcumin-loaded AQ prepared with sucrosecoated HAP showed endothermic peaks at 451°C. The peak likely represents the melting and degradation of sucrose, curcumin, and PVP. Curcumin-loaded AQ prepared with trehalose-coated HAP showed mild endothermic peaks at 175°C and 448°C. The peaks correspond to the melting and decomposition of trehalose, curcumin, and PVP.

Similar to the results from Damera et al. (2019, 2275-4476) and Gupta et al. (2020, 7-8), stability up to high temperatures with no significant transitions was displayed by the pure HAP in this study [26, 30]. This indicates the inherent thermal stability of HAP. In this study, endothermic peaks at 142.66°C and 220°C were exhibited by lactose-coated HAP, corresponding to the melting and decomposition of lactose. This is comparable to Chaudhary et al. (2022, 253-254), where endothermic peaks at 235°C and 241°C were shown by lactose, indicating melting and intermediate formation. Both studies reflect the thermal transitions associated with lactose [46]. Endothermic peaks at 121.52°C and 240°C were observed in maltose-coated HAP in this study, aligning with the thermal behavior of maltose observed in related studies. For instance, similar endothermic transitions indicating melting and decomposition were shown by maltose. In the results, sucrose-coated HAP showed endothermic peaks at 200°C and 220°C, which align with the melting and subsequent decomposition of sucrose. This is consistent with other studies where similar thermal transitions were noted. The thermal transitions of trehalose-coated HAP observed in this study (102.01°C, 205°C, and 309°C) agree with studies such as Goyal et al. (2008, 1303), where endothermic peaks indicated the phase transitions and degradation of trehalose [34].

The DSC results for pure curcumin in this study, showing endothermic peaks at 181°C, are consistent with the findings from Gupta et al. (2020, 7–8), where an endotherm at around 178.19°C was exhibited by curcumin [26]. This similarity underscores the crystalline nature and melting point of pure curcumin. Observation of complex thermal behavior in curcumin-loaded AQ due to interactions between curcumin, PVP, and carbohydrate coatings was made in this study, comparable to the findings from Gupta et al. (2020, 7–8) [26]. Similar endothermic peaks in the range of 447°C to 451°C were noted, suggesting the combined melting and decomposition of the components. The inherent properties of materials such as HAP, lactose, maltose, sucrose, trehalose, and curcumin dictate their thermal behavior. The

consistent observation of endothermic and exothermic peaks at specific temperatures across different studies underscores the reproducibility of these thermal properties. Variations in formulation techniques, such as the method of coating and the interaction between components, can result in slight shifts in peak temperatures. For instance, the interaction between curcumin and PVP in curcumin-loaded AQ can lead to different thermal behaviors.

4.4 | In Vitro Drug Release Studies

The dissolution studies were carried out to evaluate the release profiles of curcumin from AQ formulated with different carbohydrate carriers: trehalose, maltose, sucrose, and lactose. The studies were conducted in two distinct media: HCl at pH 1.2 to simulate gastric fluid and PBS at pH 7.4 to mimic physiological conditions.

Figure 9 shows the dissolution study in the acidic environment of HCl at pH 1.2, and the curcumin loaded onto trehalose, maltose, sucrose, and lactose AQ released over 80% in 90 min. In contrast, the pure drug exhibited a rapid initial release, reaching approximately 20% dissolution within the first 100 min and plateauing after that. This stark difference suggests that the carbohydrate carriers significantly modulated the release rate of curcumin.

In the PBS medium at pH 7.4, all aquasome formulations displayed a similar trend, with more drug release than pure drugs, as shown in Figure 10. Notably, the trehalose AQ showed a slightly delayed release profile compared to other carbohydrates, which could indicate its potential for prolonged drug release in the systemic circulation.

Table 5 shows the linear correlation coefficients for in vitro release data from various models. A higher r^2 value indicates a better fit of the model to the experimental data. The model with the highest r^2 value is generally considered the most appropriate.

As expected, a first-order release was observed for free curcumin and curcumin-loaded AQ. The drug was completely released within 6–8 h. The release of curcumin from the AQ was concentration-dependent.

The Higuchi model typically describes drug release as a square root of time, indicating diffusion-controlled release mechanisms. The R^2 values for curcumin-loaded AQ-lactose (0.9274) and AQ-sucrose (0.8417) suggest a good fit, indicating significant diffusion control in these cases. However, the first-order release had a higher model fitness.

Zero-order and Hixson–Crowell models generally showed poorer fits across the board, particularly evident in curcumin-loaded AQ-maltose and pure curcumin for the Hixson–Crowell model. This might suggest that these models, which are more indicative of systems where the drug release rate is constant (zero order) or modified by changes in the surface area and diameter of particles (Hixson–Crowell), are less suitable for describing the release profiles from AQ.

TABLE 5 | Linear correlation coefficients obtained for in vitro release data from various models.

Formulation			Equations and r^2		
Model	Zero-order	First order	Higuchi	Hixson-Crowell	Korsmeyer-Peppas
Curcumin- loaded AQ-lactose	$Y = 0.1647x + 37.196$ $R^2 = 0.7838$	$y = 16.657 \ln(x) - 6.4441$ $R^2 = 0.9451$	$y = 4.4235x + 15.655$ $R^2 = 0.9274$	$y = 0.0048x + 2.9489$ $R^2 = 0.434$	$y = 11.231\ln(x) + 14.283$ $R^2 = 0.8158$
Curcumin- loaded AQ-maltose	$y = 0.1226x + 57.7$ $R^2 = 0.405$	$y = 13.689 \ln(x) + 23.419$ $R^2 = 0.9035$	$y = 3.4703x + 41.538$ $R^2 = 0.6342$	$y = 0.0034x + 3.528$ $R^2 = 0.2167$	$y = 15.743\ln(x) + 14.054$ $R^2 = 0.8479$
Curcumin- loaded AQ-sucrose	$y = 0.1368x + 48.313$ $R^2 = 0.6709$	$y = 14.982\ln(x) + 7.4375$ $R^2 = 0.9494$	$y = 3.9839x + 26.531$ $R^2 = 0.8417$	$y = 0.004x + 3.2296$ $R^2 = 0.3302$	$y = 11.231\ln(x) + 14.283$ $R^2 = 0.8158$
Curcumin- loaded AQ-trehalose	$y = 5.4823x + 17.312$ $R^2 = 0.7973$	$41.628\ln(x) - 14.057$ $R^2 = 0.9465$	$y = 2.8732x + 51.993$ $R^2 = 0.6137$	$y = 0.0033x + 3.5746$ $R^2 = 0.2094$	$y = 15.743\ln(x) + 16.054$ $R^2 = 0.8479$
Pure curcumin	$y = 0.0442x + 23.664$ $R^2 = 0.5645$	$y = 2.9399 \ln(x) + 19.505$ $R^2 = 0.7718$	$y = 1.1002x + 19.252$ $R^2 = 0.6849$	•	$y = 2.9399 \ln(x) + 19.505$ $R^2 = 0.7718$

TABLE 6 Stability studies of curcumin-loaded AQ for 3 months at 25°C \pm 1°C/60% RH \pm 2% RH.

Formulation			Duration		
	7 days	14 days	30 days	2 months	3 months
Curcumin loaded AQ-lact	ose				
Curcumin % content	99.97 ± 1.2	99.90 ± 1.3	100.00 ± 1.0	99.95 ± 1.4	99.90 ± 1.0
Particle size	317.8 ± 10.2	326.7 ± 12.4	340.2 ± 15.0	324.0 ± 11.8	362.8 ± 14.7
Zeta potential	-22.0 ± 0.3	-21.8 ± 0.4	-22.6 ± 0.5	-20.3 ± 0.4	-20.6 ± 0.5
PDI	0.576 ± 0.25	0.571 ± 0.20	0.553 ± 0.18	0.531 ± 0.17	0.505 ± 0.15
Visual inspection	Pass	Pass	Pass	Pass	Pass
Curcumin loaded AQ-mal	tose				
Curcumin % content	100.30 ± 1.1	98.4 ± 2.2	99.7 ± 2.1	98.5 ± 1.2	99.8 ± 0.4
Particle size	326.7 ± 12.3	335.2 ± 14.1	307.8 ± 10.4	374.7 ± 15.6	341.4 ± 13.2
Zeta potential	-20.9 ± 0.3	-20.8 ± 0.4	-20.8 ± 0.4	-22.1 ± 0.5	-20.7 ± 0.3
PDI	0.476 ± 0.20	0.495 ± 0.22	0.503 ± 0.21	0.463 ± 0.18	0.494 ± 0.20
Visual inspection	Pass	Pass	Pass	Pass	Pass
Curcumin loaded AQ-suci	rose				
Curcumin % content	99.1 ± 1.4	98.5 ± 2.8	98.5 ± 1.8	99.1 ± 3.2	98.6 ± 0.3
Particle size	223.1 ± 9.4	215.2 ± 8.8	216.0 ± 9.1	229.6 ± 10.2	257.0 ± 12.5
Zeta potential	-21.4 ± 0.4	-21.6 ± 0.5	-22.4 ± 0.6	-20.5 ± 0.4	-21.2 ± 0.5
PDI	0.560 ± 0.21	0.571 ± 0.22	0.523 ± 0.20	0.599 ± 0.24	0.550 ± 0.21
Visual inspection	Pass	Pass	Pass	Pass	Pass
Curcumin loaded AQ-treh	alose				
Curcumin % content	99.3 ± 0.2	98.1 ± 0.7	99.3 ± 2.8	98.7 ± 1.3	98.9 ± 0.1
Particle size	322.6 ± 11.8	330.6 ± 12.4	330.5 ± 12.3	318.5 ± 11.6	342.7 ± 13.1
Zeta potential	-21.7 ± 0.4	-20.8 ± 0.3	-21.8 ± 0.4	-20.1 ± 0.4	-20.7 ± 0.3
PDI	0.489 ± 0.21	0.490 ± 0.22	0.495 ± 0.23	0.503 ± 0.22	0.505 ± 0.22
Visual inspection	Pass	Pass	Pass	Pass	Pass

Note: Values are reported as mean \pm SD.

Dissolution Study in HCl at PH 1.2

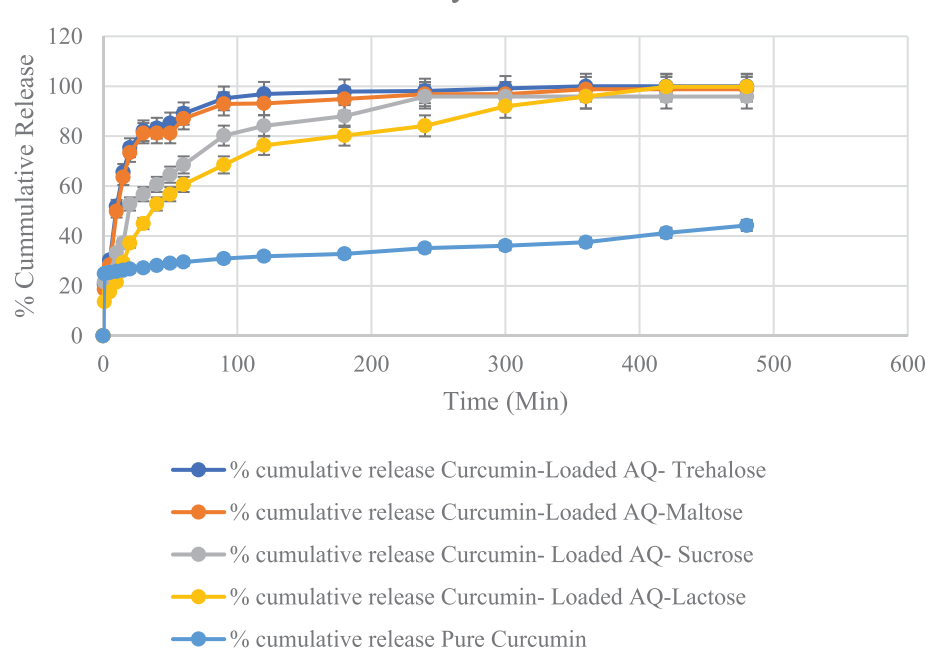


FIGURE 9 | In vitro dissolution at 1.2 pH.

Dissolution study in Phosphate Buffer Saline at 7.4

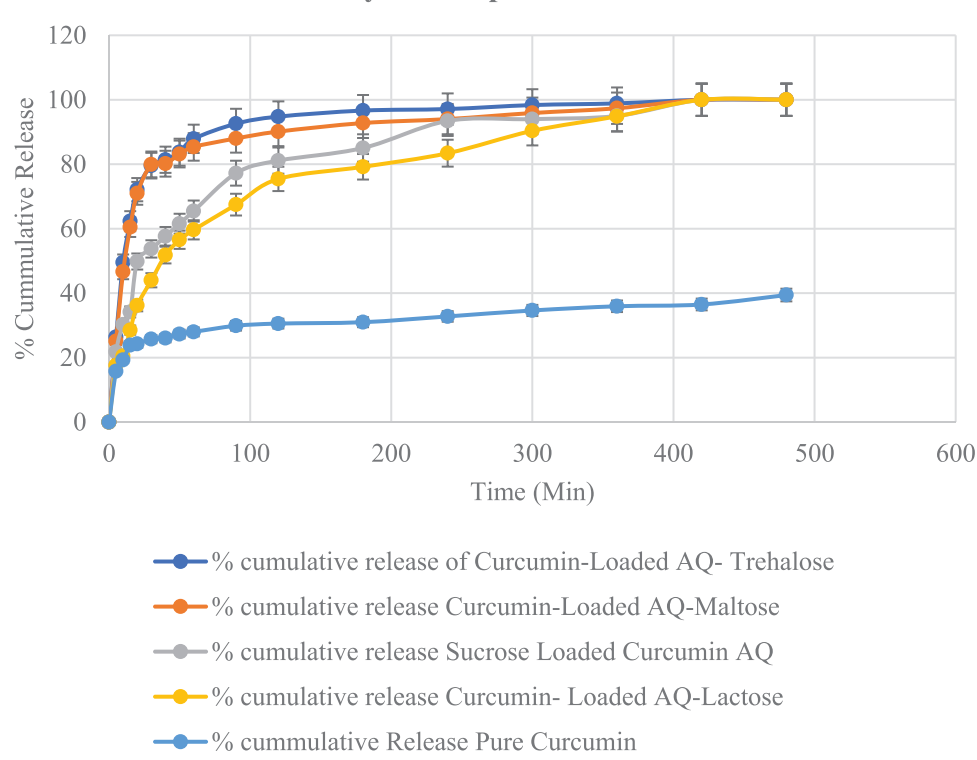


FIGURE 10 | In vitro, pure and curcumin-loaded AQ release profiles in phosphate buffer solution, pH 7.4.

The observed dissolution profiles suggest that the encapsulation of curcumin within AQ markedly improves its release kinetics. The release profiles observed for the carbohydrate-loaded AQ could be attributed to the multilayered structure of AQ, which provides a barrier to the immediate release of the encapsulated drug.

Incorporating different carbohydrates into the aquasome matrix appears to influence the drug release rate, possibly due to the varying molecular interactions between curcumin and the carbohydrate carriers. Trehalose, in particular, might enhance the stability of curcumin, given its known protective properties for biomolecules.

TABLE 7 Stability studies of curcumin-loaded AQ for 3 months at 4° C \pm 3° C/60% RH \pm 2% RH.

Formulation			Duration		
	7 days	14 days	30 days	2 months	3 months
Curcumin loaded AQ-lacto	se				
Curcumin % content	97.8 ± 2.7	98.2 ± 1.6	98.7 ± 2.7	99.97 ± 1.2	98.1 ± 0.5
Particle size	320.3 ± 10.8	339.6 ± 11.5	340.2 ± 12.0	329.7 ± 11.2	332.6 ± 11.8
Zeta potential	-21.8 ± 0.4	-21.5 ± 0.3	-20.9 ± 0.4	-20.7 ± 0.3	-24.0 ± 0.5
PDI	0.576 ± 0.22	0.538 ± 0.21	0.533 ± 0.20	0.543 ± 0.21	0.530 ± 0.20
Visual inspection	Pass	Pass	Pass	Pass	Pass
Curcumin loaded AQ-malt	ose				
Curcumin % content	97.2 ± 3.6	99.1 ± 1.5	99.5 ± 2.0	99.2 ± 3.4	99.1 ± 0.5
Particle size	328.1 ± 12.1	358.4 ± 13.5	318.8 ± 11.4	322.1 ± 11.6	355.8 ± 13.1
Zeta potential	-20.8 ± 0.4	-20.7 ± 0.3	-20.4 ± 0.3	-20.7 ± 0.4	-20.4 ± 0.3
PDI	0.473 ± 0.20	0.501 ± 0.21	0.593 ± 0.24	0.521 ± 0.22	0.598 ± 0.25
Visual inspection	Pass	Pass	Pass	Pass	Pass
Curcumin loaded AQ-sucro	ose				
Curcumin % content	96.6 ± 3.2	98.5 ± 0.9	98.9 ± 1.7	98.4 ± 2.5	99.4 ± 0.6
Particle size	215.5 ± 9.2	225.1 ± 10.1	236.2 ± 11.0	235.3 ± 10.8	220.3 ± 9.7
Zeta potential	-20.9 ± 0.4	-20.7 ± 0.3	-20.4 ± 0.3	-20.3 ± 0.3	-20.1 ± 0.3
PDI	0.474 ± 0.20	0.482 ± 0.21	0.476 ± 0.20	0.614 ± 0.25	0.409 ± 0.18
Visual inspection	Pass	Pass	Pass	Pass	Pass
Curcumin loaded AQ-treha	alose				
Curcumin % content	99.1 ± 1.6	99.8 ± 3.1	99.1 ± 0.6	98.7 ± 3.1	99.0 ± 1.0
Particle size	268.8 ± 10.7	290.0 ± 11.6	340.2 ± 13.5	322.7 ± 12.8	348.6 ± 14.0
Zeta potential	-21.9 ± 0.4	-21.1 ± 0.3	-22.6 ± 0.5	-23.5 ± 0.6	-20.8 ± 0.3
PDI	0.503 ± 0.21	0.482 ± 0.20	0.510 ± 0.22	0.500 ± 0.21	0.516 ± 0.22
Visual inspection	Pass	Pass	Pass	Pass	Pass

Note: Values are reported as mean \pm SD.

The initial burst release observed with the pure drug in acidic conditions suggests its rapid dissolution and potential for quick absorption in the gastric environment. A curcumin-loaded amorphous calcium phosphate nanoparticle study also found a first-order kinetic model for releasing curcumin [25].

4.5 | Stability Studies

4.5.1 | Long Term Stability

Curcumin-loaded AQ were stored at two conditions: $4^{\circ}\text{C} \pm 1^{\circ}\text{C}/60\%$ RH $\pm 2\%$ and $25^{\circ}\text{C} \pm 1^{\circ}\text{C}/60\%$ RH $\pm 2\%$ for 90 days. The size, zeta potential, and curcumin content of the AQ showed no statistically significant changes (p > 0.05) under these storage conditions. See Tables 6 and 7 for details.

After 3 months of storage under refrigerated conditions, curcumin-loaded AQ were found to be stable with no significant change ($p \le 0.05$) in any of the observed parameters. Similarly, curcumin-loaded AQ were stable under room temperature.

The particle size and zeta potential exhibited stability despite the varying conditions, with no significant fluctuations detected throughout the study. This suggests a robust formulation capable of withstanding moderate changes in environmental conditions without degradation or agglomeration. Such findings align with previous studies highlighting the stabilizing effects of aquasome technology on bioactive compounds [47].

Similarly, the curcumin content remained stable under both storage conditions. This observation is critical as it suggests that encapsulation in AQ effectively protects curcumin from degradation, a common challenge with this compound due to its sensitivity to light and temperature. The stability of curcumin in AQ could be attributed to the protective matrix that limits exposure to degradative environmental factors [26, 47].

This study suggests that curcumin-loaded AQ can be stored at either 4°C or 25°C without degradation. Furthermore, amber containers are recommended to maintain stability against photodegradation. These findings suggest that curcumin-loaded AQ can be distributed and stored without stringent temperature controls, reducing logistical costs and complexity [28].



FIGURE 11 | Photostability studies on various parameters of curcumin-loaded AQ and its comparison with free curcumin.

4.5.2 | Photostability

The photodegradation study (Figure 11) revealed that curcumin degraded by 4% in the amber container and 8% in the transparent container. Notably, the particle size, zeta potential, and PDI decreased significantly in the transparent container compared to the amber container. These findings suggest that the amber container offers superior protection against the photodegradation of curcumin. Additionally, compared to curcumin loaded in AQ, the latter demonstrated enhanced protective effects against degradation, as evidenced by the data presented in the above graphs. This indicates that AQ are an effective medium for preserving the integrity of curcumin under exposure to light.

Particle size increased from the 0th day to the 14th day for the transparent condition, indicating a possible agglomeration or growth of particles. The amber condition also showed an increase but not as pronounced as the transparent condition.

There is an increase in PDI value for the transparent condition, suggesting a broader size distribution and less uniformity among

particles. Amber's condition also showed a slight increase. Minor changes are observed in zeta potential, with a slight increase in both storage conditions, which might affect stability. TDC remained stable at 300 for the 0th and 14th day amber conditions, with a negligible decrease for the transparent condition. EE remained constant for amber and transparent conditions on the 14th day.

Upon exposure to light, there was an observable increase in particle size and PDI, alongside a decrease in zeta potential. These changes could be ascribed to the kinetic energy conferred to the particles by the light, which may enhance the frequency and intensity of interparticle collisions, leading to aggregation. A study investigating curcumin-encapsulated lipidic nano constructs observed similar trends [26]. Amber containers exhibited a smaller decline in zeta potential and TDC and a lesser increase in PDI and particle size than transparent containers. Consequently, amber containers may offer superior protection against the photodegradation of curcumin, making them a more suitable choice for storage to preserve the compound's integrity.

4.6 | Biocompatibility Studies

The hemolysis assay was used to measure the extent to which the AQ damaged RBCs. This assay provided valuable information on the biocompatibility of the drug-loaded AQ and helped to evaluate their potential toxicity.

The hemolysis percentages for curcumin-loaded aquasome formulations (Figure 13) demonstrated varied yet clinically acceptable levels of biocompatibility. Curcumin-loaded AQ-lactose exhibited hemolysis percentages ranging from 1.87% to 3.55%, showing a decreasing trend with increasing concentration. The hemolysis percentage varied between 1.96% and 3.43% for curcumin-loaded AQ-maltose, with fluctuations across different concentrations. The curcumin-loaded AQ-sucrose formulation showed the highest hemolysis at 3.88% at a 1:1 concentration, significantly decreasing to 0.62% at a 1:60 concentration. Curcumin-loaded AQ-trehalose had hemolysis percentages ranging from 0.98% to 3.05%, with a notable drop at higher concentrations. Pure curcumin consistently exhibited the lowest hemolysis percentages, ranging from 0.41% to 0.72%, confirming its biocompatibility. These results indicate that while there are some variations, all formulations remain within safe limits for clinical use. Among the disaccharide-based AQ, those loaded with sucrose exhibited the highest hemolysis at lower concentrations but reduced significantly at higher dilutions. A general trend of decreasing hemolysis percentage with increasing concentration was observed, particularly for lactose and sucrose-based formulations. This suggests a concentration-dependent biocompatibility. where higher dilution reduces cytotoxic effects.

Under light microscopy, Triton X-100 treated samples showed significant hemolysis, confirming its role as a positive control. Very little hemolysis was observed in samples treated with pure curcumin and curcumin-loaded AQ, corroborating the spectrophotometric findings as shown in Figure 12. These formulations are safe and exhibit negligible hemolytic activity, as the percentage of hemolysis is consistently below 5%, rendering them clinically favorable [30]. The results of this study are similar to another study which found less than 2% for the hemolysis test [48].

5 | Conclusion

This study formulated and characterized curcumin-loaded AQ to enhance the drug delivery of poorly soluble curcumin. Utilizing HAP cores coated with disaccharides—sucrose, maltose, lactose, and trehalose—and PVP as a hydrophilic carrier, the AQ significantly improved curcumin's solubility and stability. Optimization through a QbD approach yielded a high desirability coefficient (0.8385), indicating that variables like core-to-coat ratio, incubation time, and drug amount critically influenced particle size, PDI, and zeta potential.

Characterization revealed increased particle sizes for sugarcoated HAP and curcumin-loaded AQ, with lactose coatings offering moderate stability. Encapsulation efficiencies peaked at 53.67% for formulations with trehalose and lactose. Analytical techniques such as EDX and XRD confirmed successful sugar coating and curcumin loading, while TGA and DSC analyses highlighted the importance of disaccharide selection for ther-

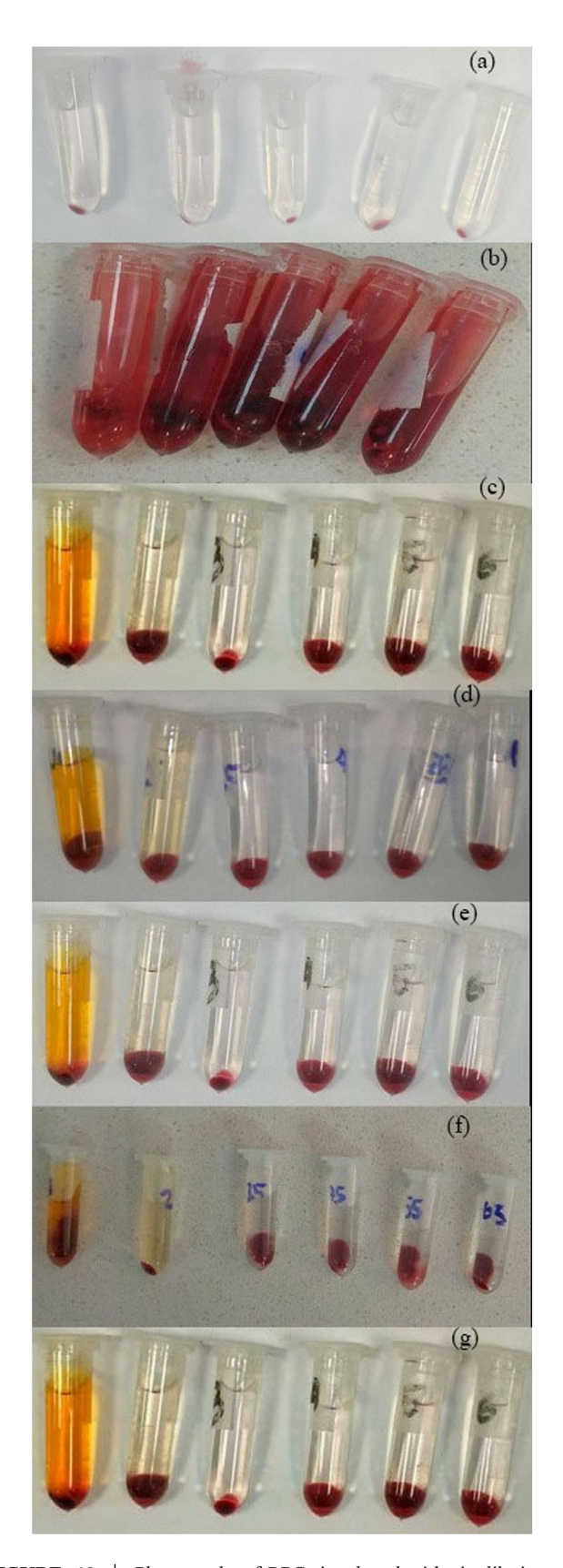


FIGURE 12 | Photographs of RBCs incubated with six dilutions of curcumin-loaded AQ. Triton X 100 (+) and 0.9% saline (-) are positive and negative controls, respectively. (a) 0.9% saline (negative control), (b) Triton X 100 (positive control) pure curcumin, (d) curcumin-loaded AQ-lactose, (e) curcumin-loaded AQ-maltose, (f) curcumin-loaded AQ-trehalose (g) curcumin-loaded AQ-sucrose.

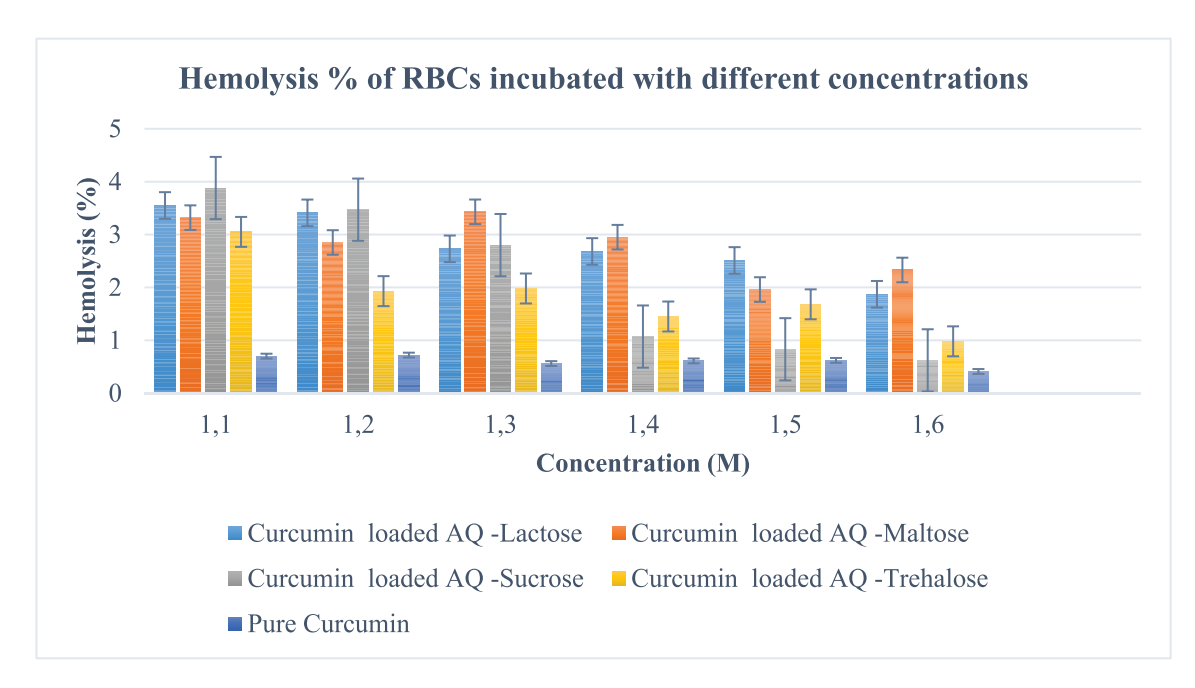


FIGURE 13 | Hemolysis % of RBCs incubated with different concentrations of pure curcumin and aquasome formulations.

mal stability, showing unique decomposition temperatures and weight loss patterns.

In vitro release studies demonstrated a sustained, first-order release profile of curcumin in both acidic and physiological conditions, outperforming the pure drug. Stability assessments over 3 months showed no significant changes in key parameters, affirming formulation robustness, while photostability tests recommended amber containers to prevent degradation. Biocompatibility evaluations indicated minimal hemolytic activity, underscoring clinical safety.

Further, in vivo studies are necessary to evaluate the pharmacokinetics and therapeutic efficacy fully. Future research could investigate the delivery of other poorly soluble drugs using aquasome technology.

Acknowledgments

We want to thank Liban Barre for his guidance on the QbD approach and the development of the research idea. We are also thankful to the Department of Pharmaceutical Technology at Anadolu University for providing some of the materials used in the study as well as the laboratory.

Ethics Statement

The animal experimental part of this research was prepared according to the guidelines of the Committee for Control and Supervision of Experiments on Animals. The experimental protocol was approved by Anadolu University Animal Experiments Ethics Committee protocol no: 2024-13.

Conflicts of Interest

The authors declare no conflicts of interest.

Data Availability Statement

The authors declare that all data are available within the article and other related data are available in supporting information and upon request.

References

- 1. M. L. Del Prado-Audelo, I. H. Caballero-Florán, J. A. Meza-Toledo, et al., "Formulations of Curcumin Nanoparticles for Brain Diseases," *Biomolecules* 9, no. 2 (2019): 56, https://doi.org/10.3390/biom9020056.
- 2. S.-I. Sohn, A. Priya, B. Balasubramaniam, et al., "Biomedical Applications and Bioavailability of Curcumin-An Updated Overview," *Pharmaceutics* 13, no. 12 (2021): 2102, https://doi.org/10.3390/pharmaceutics13122102.
- 3. V. S. Ipar, A. Dsouza, and P. V. Devarajan, "Enhancing Curcumin Oral Bioavailability Through Nanoformulations," *European Journal of Drug Metabolism and Pharmacokinetics* 44, no. 4 (2019): 459–480, https://doi.org/10.1007/s13318-019-00545-z.
- 4. P. Anand, A. B. Kunnumakkara, R. A. Newman, and B. B. Aggarwal, "Bioavailability of Curcumin: Problems and Promises," *Molecular Pharmaceutics* 4, no. 6 (2007): 807–818, https://doi.org/10.1021/mp700113r.
- 5. H. Michal, F. v. G. Rowan, B. Mans, and C. M. Martin, "The Molecular Basis for the Pharmacokinetics and Pharmacodynamics of Curcumin and Its Metabolites in Relation to Cancer," *Pharmacological Reviews* 66, no. 1 (2014): 222, https://doi.org/10.1124/pr.110.004044.
- 6. L. Dahir, A. Kaur, A. Manocha, et al., "Aquasomes: Water like Bodies Vesicular System for Therapeutics Molecules as Robust System for Delivery," *European Journal of Molecular and Clinical Medicine* 7, no. 7 (2020): 2585–2607.
- 7. S. S. Jain, P. S. Jagtap, N. M. Dand, K. R. Jadhav, and V. J. Kadam, "Aquasomes: A Novel Drug Carrier," *Journal of Applied Pharmaceutical Science* 2, no. 1 (2012): 184–192.
- 8. M. H. Asfour, "Advanced Trends in Protein and Peptide Drug Delivery: A Special Emphasis on Aquasomes and Microneedles Techniques," *Drug Delivery and Translational Research* 11, no. 1 (2021): 1–23, https://doi.org/10.1007/s13346-020-00746-z.
- 9. S. Banerjee and K. K. Sen, "Aquasomes: A Novel Nanoparticulate Drug Carrier," *Journal of Drug Delivery Science and Technology* 43 (2018): 446–452, https://doi.org/10.1016/j.jddst.2017.11.011.

- 10. N. Kossovsky, R. F. Bunshah, A. Gelman, et al., "A Nondenaturing Solid Phase Pharmaceutical Carrier Comprised of Surface-Modified Nanocrystalline Materials," *Journal of Applied Biomaterials* 1, no. 4 (1990): 289–294, https://doi.org/10.1002/jab.770010404.
- 11. N. Kossovsky, A. Gelman, H. J. Hnatyszyn, et al., "Surface-Modified Diamond Nanoparticles as Antigen Delivery Vehicles," *Bioconjugate Chemistry* 6, no. 5 (1995): 507–511.
- 12. N. Kossovsky, A. Gelman, S. Rajguru, et al., "Control of Molecular Polymorphisms by a Structured Carbohydrate/Ceramic Delivery Vehicle Aquasomes," *Journal of Controlled Release* 39, no. 2 (1996): 383–388, https://doi.org/10.1016/0168-3659(95)00169-7.
- 13. N. Kossovsky, A. Gelman, E. E. Sponsler, et al., "Surface-Modified Nanocrystalline Ceramics for Drug Delivery Applications," *Biomaterials* 15, no. 15 (1994): 1201–1207, https://doi.org/10.1016/0142-9612(94)90270-4.
- 14. S. Rewar, "A Systematic Review on Aquasome's as Novel Carrier Approach," *International Journal of Analytical, Pharmaceutical and Biomedical Sciences* 4 (2015): 44–49.
- 15. M. S. Umashankar, R. K. Sachdeva, and M. Gulati, "Aquasomes: A Promising Carrier for Peptides and Protein Delivery," *Nanomedicine: Nanotechnology, Biology and Medicine* 6, no. 3 (2010): 419–426, https://doi.org/10.1016/j.nano.2009.11.002.
- 16. L. X. Yu, G. Amidon, M. A. Khan, et al., "Understanding Pharmaceutical Quality by Design," *The AAPS Journal* 16, no. 4 (2014): 771–783, https://doi.org/10.1208/s12248-014-9598-3.
- 17. D. C. Montgomery, *Design and Analysis of Experiments*. 2nd ed. (Hoboken, NJ: Arizona State University, John Wiley & Sons, 2017).
- 18. R. H. Myers, D. C. Montgomery, and C. M. Anderson-Cook, *Response Surface Methodology: Process and Product Optimization Using Designed Experiments* (Hoboken, NJ: John Wiley & Sons, 2016).
- 19. S. Beg and M. S. Hasnain, *Pharmaceutical Quality by Design: Principles and Applications* (Cambridge, MA: Academic Press, 2019).
- 20. K. Kaur, P. Kush, R. S. Pandey, J. Madan, U. K. Jain, and O. P. Katare, "Stealth Lipid Coated Aquasomes Bearing Recombinant Human Interferon-α-2b Offered Prolonged Release and Enhanced Cytotoxicity in Ovarian Cancer Cells," *Biomedicine & Pharmacotherapy* 69 (2015): 267–276, https://doi.org/10.1016/j.biopha.2014.12.007.
- 21. D. P. Vengala, R. Vanamala, C. V. S. Subrahmanyam, "Carbohydrate Stabilized Ceramic Nanoparticles for the Delivery of a Poorly Soluble Drug, Lornoxicam," *Asian Journal of Pharmaceutics* 11, no. 03 (2017), 497–503, https://doi.org/10.22377/ajp.v11i03.1450.
- 22. I. Rojas-Oviedo, R. A. Salazar-López, J. Reyes-Gasga, and C. T. Quirino-Barreda, "Elaboration and Structural Analysis of Aquasomes Loaded with Indomethacin," *European Journal of Pharmaceutical Sciences* 32, no. 3 (2007): 223–230, https://doi.org/10.1016/j.ejps.2007.07.008.
- 23. P. Vengala, S. Aslam, and C. V. S. Subrahmanyam, "Development and In Vitro Evaluation of Ceramic Nanoparticles of Piroxicam," *Latin American Journal of Pharmacy* 32, no. 8 (2013): 1124–1130.
- 24. P. Vengala, S. Dintakurthi, and C. V. S. Subrahmanyam, "Lactose Coated Ceramic Nanoparticles for Oral Drug Delivery," *Journal of Pharmacy Research* 7, no. 6 (2013): 540–545, https://doi.org/10.1016/j.jopr.2013. 06.015.
- 25. X. Guo, W. Li, H. Wang, et al., "Preparation, Characterization, Release and Antioxidant Activity of Curcumin-Loaded Amorphous Calcium Phosphate Nanoparticles," *Journal of Non-Crystalline Solids* 500 (2018): 317–325, https://doi.org/10.1016/j.jnoncrysol.2018.08.015.
- 26. T. Gupta, J. Singh, S. Kaur, S. Sandhu, G. Singh, and I. P. Kaur, "Enhancing Bioavailability and Stability of Curcumin Using Solid Lipid Nanoparticles (CLEN): A Covenant for Its Effectiveness," *Frontiers in Bioengineering and Biotechnology* 8 (2020): 879, https://doi.org/10.3389/fbioe.2020.00879.
- 27. F.-L. Yen, T.-H. Wu, C.-W. Tzeng, L.-T. Lin, and C.-C. Lin, "Curcumin Nanoparticles Improve the Physicochemical Properties of Curcumin

- and Effectively Enhance Its Antioxidant and Antihepatoma Activities," *Journal of Agricultural and Food Chemistry* 58, no. 12 (2010): 7376–7382, https://doi.org/10.1021/jf100135h.
- 28. S. Kumar, S. Mohd Aquil, and A. Gupta, "Formulation and Evaluation of Voriconazole Loaded Aquasomes for the Treatment of Fungal Infection," *NeuroQuantology* 20, no. 11 (2022): 1212–1233, https://doi.org/10.14704/nq.2022.20.11.NQ66115.
- 29. L. M. Hussein Ali, A. M. Dawaba, and S. A. El-Adawy, "Formulation, Optimization and Full Characterization of Mirtazapine Loaded Aquasomes: A New Technique to Boost Antidepressant Effects," *Drug Development and Industrial Pharmacy* 50 (2024): 1–27, https://doi.org/10.1080/03639045.2024.2313538.
- 30. D. P. Damera, S. Kaja, L. S. L. Janardhanam, S. Alim, V. V. K. Venuganti, and A. Nag, "Synthesis, Detailed Characterization, and Dual Drug Delivery Application of BSA Loaded Aquasomes," *ACS Applied Bio Materials* 2, no. 10 (2019): 4471–4484, https://doi.org/10.1021/acsabm. 9b00635.
- 31. Y.-S. Lin and C. L. Haynes, "Impacts of Mesoporous Silica Nanoparticle Size, Pore Ordering, and Pore Integrity on Hemolytic Activity," *Journal of the American Chemical Society* 132, no. 13 (2010): 4834–4842, https://doi.org/10.1021/ja910846q.
- 32. S. K. Prajapati, P. Kesharwani, N. Mody, A. Jain, and S. Sharma, "Formulation by Design (FbD): An Emerging Approach to Design Vesicular Nanocarriers," in: *Micro- and Nanotechnologies-Based Product Development*, eds. N. K. Mehra and A. Gulbake (Boca Raton, FL: CRC Press, 2021), 15–31.
- 33. A. L. Azhar, A. Ma'amor, N. M. Julkapli, N. A. Sairi, and A. S. Noraizat, "Ultraviolet-Activated Clamshell Hydroxyapatite-Substituted Palladium in the Photoreduction of Methyl Orange Water Pollutant," *Turkish Journal of Chemistry* 47, no. 3 (2023): 527–539, https://doi.org/10.55730/1300-0527.
- 34. A. K. Goyal, K. Khatri, N. Mishra, et al., "Aquasomes—A Nanoparticulate Approach for the Delivery of Antigen," *Drug Development and Industrial Pharmacy* 34, no. 12 (2008): 1297–1305, https://doi.org/10.1080/03639040802071661.
- 35. K. M. Koczkur, S. Mourdikoudis, L. Polavarapu, and S. E. Skrabalak, "Polyvinylpyrrolidone (PVP) in Nanoparticle Synthesis," *Dalton Transactions* 44, no. 41 (2015): 17883–17905, https://doi.org/10.1039/C5DT02964C.
- 36. A. Rónavári, P. Bélteky, E. Boka, et al., "Polyvinyl-Pyrrolidone-Coated Silver Nanoparticles—The Colloidal, Chemical, and Biological Consequences of Steric Stabilization Under Biorelevant Conditions," *International Journal of Molecular Sciences* 22, no. 16 (2021): 8673, https://doi.org/10.3390/ijms22168673.
- 37. A. Kumar and C. K. Dixit (2017). "3 Methods for Characterization of Nanoparticles," in *Advances in Nanomedicine for the Delivery of Therapeutic Nucleic Acids*, eds. S. Nimesh, R. Chandra, and N. Gupta (Sawston, UK: Woodhead Publishing, 2017), 43–58.
- 38. S. Kommineni, S. Ahmad, P. Vengala, and C. V. S. Subramanyam, "Sugar Coated Ceramic Nanocarriers for the Oral Delivery of Hydrophobic Drugs: Formulation, Optimization and Evaluation," *Drug Development and Industrial Pharmacy* 38, no. 5 (2012): 577–586, https://doi.org/10.3109/03639045.2011.617884.
- 39. Y. Zhang and J. Lu, "A Simple Method to Tailor Spherical Nanocrystal Hydroxyapatite at Low Temperature," *Journal of Nanoparticle Research* 9, no. 4 (2007): 589–594, https://doi.org/10.1007/s11051-006-9177-3.
- 40. P. Thakare, B. Chellampillai, V. Kuvar, V. Shinde, and A. Mali, "Exploring the Potential of Three-Layered Self-Assembled Biomaterial-Based Dry Powder Inhaler for Enhanced Structural Integrity and Lung Deposition of Bioactive Lysozyme," *BioNanoScience* 14 (2024): 3341–3354.
- 41. A. Michelot, S. Sarda, C. Audin, et al., "Spectroscopic Characterisation of Hydroxyapatite and Nanocrystalline Apatite with Grafted Aminopropyltriethoxysilane: Nature of Silane–Surface Interaction," *Journal of Materials Science* 50, no. 17 (2015): 5746–5757, https://doi.org/10.1007/s10853-015-9122-x.

- 42. G. E. Poinern, R. K. Brundavanam, N. Mondinos, and Z.-T. Jiang, "Synthesis and Characterisation of Nanohydroxyapatite Using an Ultrasound Assisted Method," *Ultrasonics Sonochemistry* 16, no. 4 (2009): 469–474, https://doi.org/10.1016/j.ultsonch.2009.01.007.
- 43. F. X. Webster and D. J. Kiemle, *Spectrometric Identification of Organic Compounds* (Hoboken, NJ: John Wiley & Sons, 2005).
- 44. H. Van Nong, L. X. Hung, P. N. Thang, et al., "Fabrication and Vibration Characterization of Curcumin Extracted from Turmeric (*Curcuma longa*) Rhizomes of the Northern Vietnam," *SpringerPlus* 5, no. 1 (2016): 1147, https://doi.org/10.1186/s40064-016-2812-2.
- 45. Y. Jafari, H. Sabahi, and M. Rahaie, "Stability and Loading Properties of Curcumin Encapsulated in *Chlorella vulgaris*," *Food Chemistry* 211 (2016): 700–706, https://doi.org/10.1016/j.foodchem.2016.05.115.
- 46. J. S. Chaudhary, R. Gupta, S. K. Prajapati, and P. Bhardwaj, "Dithranol Loaded Aquasomes for the Control of Psoriasis: An In Vitro–Ex Vivo Assessment," *NeuroQuantology* 20, no. 15 (2022): 3011.
- 47. F. Abdulrazzaq, Aquasomes as a Drug Delivery System for Proteins and Peptides (Birmingham, UK: Aston University, 2016).
- 48. P. Thakare, B. Chellampillai, V. Kuvar, V. Shinde, and A. Mali, "Exploring the Potential of Three-Layered Self-Assembled Biomaterial-Based Dry Powder Inhaler for Enhanced Structural Integrity and Lung Deposition of Bioactive Lysozyme," *BioNanoScience* 14 (2024): 3341–3354, https://doi.org/10.21203/rs.3.rs-3867336/v1.

Supporting Information

 $\label{lem:conditional} Additional supporting information can be found online in the Supporting Information section.$